The lnc-FANCI-2 intrinsically restricts RAS signaling in HPV16-infected cervical cancer

Haibin Liu[1a,b], Lulu Yu[1a], Vladimir Majerciak[1], Thomas Meyer[2], Ming Yi[3], Peter F. Johnson[4], Maggie Cam[2], Douglas R. Lowy[5], and Zhi-Ming Zheng[1]*

[1]Tumor Virus RNA Biology Section, HIV Dynamics and Replication Program, CCR/NCI/NIH

[2]Collaborative Bioinformatics Resource, CCR/NCI/NIH

[3]NCI RAS Initiative, Cancer Research Technology Program, Frederick National Laboratory for Cancer Research, Frederick, MD, USA.

[4]Mouse Cancer Genetics Program, CCR/NCI/NIH

[5]Laboratory of Cellular Oncology, CCR/NCI/NIH

[a]*Co-first authors*

Running title: lnc-FANCI-2 regulates RAS signaling

[b]Present address: Center for Emerging Infectious Diseases, Wuhan Institute of Virology, and Center for Biosafety Mega-Science, Chinese Academy of Sciences, Wuhan, Hubei, 430207, China

*Corresponding: zhengt@exchange.nih.gov

ABSTRACT

We recently discovered the expression of a long noncoding RNA, lnc-FANCI-2, coinciding with cervical lesion progression from CIN1, CIN2-3 to cervical cancer. Viral E7 of high-risk HPVs and host transcription factor YY1 are two major factors promoting lnc-FANCI-2 expression. To explore possible roles of lnc-FANCI-2 in HPV-induced cervical carcinogenesis, we ablated the expression of *lnc-FANCI-2* in the HPV16-positive cervical cancer cell line, CaSki. Knock-out (KO) single cell clones expressed HPV16 oncogenes normally but displayed altered cell morphology and proliferation when compared with the parental cells. Proteomic profiling of cytosolic and secreted proteins from the parental and KO cells showed that lnc-FANCI-2 regulates expression of a subset of cell soluble receptors responsible for cell signaling, epithelial mesenchymal transition, and IFN responses. RNA-seq analyses revealed that, relative to the parental cells, lnc-FANCI-2 KO cells exhibited significantly increased RAS signaling but decreased IFN pathways. In the KO cells, phosphorylated Akt and Erk1/2, two important RAS pathway effectors, were increased more than 3-fold, accompanied by increase of IGFBP3, MCAM, VIM, and CCND2 (cyclin D2) and decrease of RAC3 expression. High levels of lnc-FANCI-2 and lower levels of MCAM in cervical cancer patients are associated with improved survival. We found that lnc-FANCI-2 interacts specifically with 32 host proteins, including H13, HNRH1, K1H1, MAP4K4, and RNPS1, and knockdown of MAP4K4 in CaSki cells led to an increase of phosphorylation of Erk1/2 and somewhat Akt. In summary, a key function of lnc-FANCI-2 is to intrinsically regulate RAS signaling to impact cervical lesion progression and affect cervical cancer prognosis.

44 **Significance**

45 Expression of lnc-FANCI-2 is related to cervical lesion progression. Knock-out (KO) or knock-
46 down (KD) of lnc-FANCI-2 expression in HPV16-positive cervical cancer cells CaSki
47 significantly increases RAS signaling, phosphorylation of Akt and Erk1/2, and the epithelial
48 mesenchymal transition factors. lnc-FANCI-2 KO also regulates the expression of a subset of
49 cell soluble receptor proteins IGFBP3 and MCAM. A high level of lnc-FANCI-2 and lower level
50 of MCAM in cervical cancer patients are associated with improved survival. lnc-FANCI-2 in
51 CaSki cells interacts specifically with 32 host proteins, including MAP4K4. KD of MAP4K4
52 expression in CaSki cells led to an increase in phosphorylation of Erk1/2 and Akt. Thus, one lnc-
53 FANCI-2 function is to intrinsically regulate RAS signaling to impact cervical lesion
54 progression.

55 **INTRODUCTION**

56 Cervical cancer is a leading cause of mortality in women worldwide. It is the second most
57 diagnosed cancer among women, with an estimated 661,000 new cases worldwide each year, and
58 the third most frequent cause of cancer-related death, accounting for 348,000 deaths annually [1].
59 Persistent infections in the cervical epithelium with the cancer-associated alpha human
60 papillomaviruses (high-risk HPVs), in particular HPV16 and HPV18 with the sustained
61 expression of viral oncoproteins, E6 and E7, contribute to squamous epithelial cell tumorigenesis
62 [2-4]. Approximate 31.3% of high-grade neoplastic cervical lesions progress to invasive cervical
63 cancer in 30 years [5], while most lesions resolve spontaneously. The progression to cervical
64 cancer typically takes 15 to 20 years after initial infection (https://www.who.int/news-room/fact-
65 sheets/detail/cervical-cancer). These observations suggest that active host defense systems play
66 important roles in preventing malignant transformation of neoplastic cervical lesions, and
67 additional factors besides E6 and E7 are necessary for cervical cancer development. Indeed, one
68 tumor suppressor network, the Fanconi anemia (FA) pathway [6], can be activated by HPV-
69 induced DNA damage. FA proteins including FANCA, FANCD2 and FANCI are elevated upon
70 HPV infection [7-9] and the activated FA pathway restricts HPV replication and guards host
71 genome stability [10]. FANCD2 mutation stimulates HPV16 and HPV31 genome amplification
72 and also promotes cervical and vaginal cancer development in HPV16 E7 transgenic mouse [11,
73 12].

74 HPV-positive cervical cancer tissues in general exhibit wild-type p53, wild-type K-RAS,
75 and no overexpression of RAS genes [13-16]. Viral oncoprotein E7 plays a major role in the
76 immortalization of primary epithelial cells mainly by inactivation of pRb family of proteins [17],
77 whereas E6 mediates degradation of tumor suppressor p53 and activation of human telomerase

78 reverse transcriptase (hTERT) transcription [18-20]. However, high-risk E6 and E7 are necessary
79 but not sufficient to transform fully the immortalized cells into malignant cells [21-25] and
80 additional oncogenic stress is needed. For example, the $HRAS^{G12V}$, a constitutively activated
81 RAS GTPase mutation, triggers malignant transformation of E6/E7-expressing keratinocytes
82 [26-29]. Normal RAS regulates cell proliferation, cell differentiation and cell adhesion through
83 cellular signal transduction from growth-factor receptors such as insulin-like growth factors
84 (IGFs) and insulin-like growth factor binding proteins (IGFBP1-6) [30-32]. Thus, overactive
85 RAS signaling might facilitate transformation of E6/E7-expressing keratinocytes. In transgenic
86 mice, HPV16 E6 and E7 can promote the development of spontaneous epithelial skin tumors, but
87 not spontaneous tumors of the reproductive tract [33-36]. Prolonged estrogen treatment is
88 required [37]. Estrogen receptor (ER) activation stimulates the mitogen-activated protein kinase
89 (MAPK/Erk) and phosphoinositide 3-kinase (Pl3K/Akt) pathways, both of which are mediated
90 by RAS [38]. However, the molecular mechanism underlying estrogen-induced cervical cancer
91 in E6 and E7 transgene mice is not fully understood.

92 Long non-coding RNAs (lncRNAs) are RNAs over 200 nucleotides (nt) in length lacking
93 a coding capacity for translation into functional proteins. Although several lncRNAs have been
94 proposed to function in diverse biological processes, evidence is still lacking to support the
95 functionality of the majority of lncRNAs [39, 40].

96 We recently reported an increased level of lnc-FANCI-2 expression in high-risk HPV-
97 positive cervical intraepithelial neoplasia (CIN) and invasive cervical cancer (ICC) tissues [8].
98 At least 14 RNA isoforms of lnc-FANCI-2 are expressed by usage of two alternative promoters,
99 alternative RNA splicing, and alternative selection of two polyadenylation sites from the
100 genomic locus adjacent to the FANCI on Chr5. Ironically, the lnc-FANCI-2 was wrongly

101 annotated by NCBI as a *MIR9-3HG* in the recently updated RefSeq database
102 (https://www.ncbi.nlm.nih.gov/refseq/) and two alternative lnc-FANCI-2 promoters identified
103 for expression of lnc-FANCI-2 are ~10 kb downstream of the non-expressible miR9-3 gene [8].
104 Both lnc-FANCI-2 and FANCI are up-regulated simultaneously in neoplastic cervical lesions
105 and cervical cancer by high-risk HPV infections. E6 but, in particular E7 are responsible for the
106 enhanced expression of lnc-FANCI-2, the transcription of which is also regulated by YY1[8].
107 HPV infection increases YY1 levels but decreases the expression of p53-dependent miR-29a
108 which targets the YY1 3′ UTR. Viral E7 interacts with YY1 and facilitates YY1 transactivation
109 of lnc-FANCI-2 promoter [8]. In situ hybridization has revealed that lnc-FANCI-2 is
110 preferentially cytoplasmic, but its function in HPV infected cells has not been characterized. In
111 this report, we demonstrate that lnc-FANCI-2 in HPV16-infected cells controls RAS signaling
112 by interaction with MAP4K4 and other RNA-binding proteins. Ablation of lnc-FANCI-2 in the
113 cells promotes RAS signaling and phosphorylation of Akt and Erk. High levels of lnc-FANCI-2
114 and low level of MCAM expression in cervical cancer patients correlate with improved survival,
115 indicating that lnc-FANCI-2 plays a critical role in regulating RAS signaling to affect cervical
116 cancer progression and patient outcomes.

117 **RESULTS**

118 **Differential expression of lnc-FANCI-2 in cervical cancer tissues and its derived cell lines**
119 As lnc-FANCI-2 expression is up-regulated along with cervical lesion progression by high-risk
120 HPV infections [8], we further verified the increased expression of lnc-FANCI-2 in cervical
121 cancer tissues by RNAscope single molecule RNA *in situ* hybridization (RNA-ISH) using a lnc-
122 FANCI-2 antisense probe spanning over the major isoform of lnc-FANCI-2 nt 359-1713 region
123 (GenBank MT669800.1). We found both cytoplasmic and nuclear locations of the increased lnc-

124 FANCI-2 ISH signals within the tumor nest in HPV16-infected cervical squamous cell
125 carcinoma tissues, but not much so in its adjacent tissue areas (Fig. 1A/B). The increased
126 expression of lnc-FANCI-2 became obvious in human foreskin keratinocytes with HPV16 or
127 HPV18 infection when compared to the HFK cells without HPV infection (Fig. 1C).

128 However, we subsequently demonstrated the high expression of lnc-FANCI-2 in two
129 HPV16-infected cervical cancer cell lines (SiHa and CaSki) and two HPV16-infected low-grade
130 cervical lesion-derived cervical keratinocyte subclone lines (W12 20861 and W12 20863 cells),
131 but not in two HPV18-infected cervical cancer cell lines (HeLa and C4II cells), nor other HPV-
132 negative cell lines of HCT116 (colorectal cancer cells), BCBL-1 (body cavity B lymphoma
133 cells), HEK293 (Ad5 E1/E2-immortalized human kidney cells), and HaCaT (spontaneously
134 immortalized human epidermal cells) (Fig. S1A). Interestingly, the high expression of lnc-
135 FANCI-2 was observed in a HPV-negative cervical cancer cell line C33A cells with mutations of
136 both p53 and RB genes [41] (Fig. S1A). Northern blot confirmed the increased expression of lnc-
137 FANCI-2 in C33A cells but no expression in HeLa cells (Fig. S1B).

138 Subcellular distribution of lnc-FANCI-2 was characterized by cell fractionation and
139 Western blot assays using nuclear SRSF3 and cytoplasmic GAPDH protein as an indication of
140 fractionation efficiency (Fig. S1C). By RT-qPCR analysis of the fractionated total RNA, we
141 demonstrated that lnc-FANCI-2 RNA is mainly cytoplasmic in HPV16-positive CaSki cells, but
142 nuclear in HPV16-positive SiHa and HPV-negative C33A cells (Fig. S1C). The differential
143 subcellular distributions of lnc-FANCI-2 RNA from CaSki to SiHa and C33A cells (Fig. S1D)
144 were further confirmed by RNAscope RNA-ISH using the lnc-FANCI-2 antisense probe
145 described above.

146 **lnc-FANCI-2 regulates proliferation of HPV-transformed cervical cancer cells**

147 lnc-FANCI-2 RNA is transcribed mainly from a proximal promoter TSS2, but also from
148 an alternative minor, distal promoter TSS1. Two highly conserved YY1 binding motifs upstream
149 of the TSS2 are essential for the TSS2 transcriptional activity [8] (Fig. 2A). To elucidate the
150 function of lnc-FANCI-2 in high-risk HPV-infected cervical cancer cells, we knocked out (KO)
151 lnc-FANCI-2 expression in HPV16-positive CaSki cells using CRISPR/Cas9 deletion of either a
152 3-kb promoter region encompassing both TSS1 and TSS2 or an 86-bp region containing two
153 YY1-binding motifs in the TSS2 promoter (Fig. 2A). Two tested gRNAs with high KO
154 efficiency were selected and cloned into a modified CRISPR/Cas9 expression vector to express
155 both 5′-specific gRNA and 3'-specific gRNA simultaneously for efficient genome editing [42].
156 CaSki cells stably transfected with the dual gRNA expression vector were generated. Through a
157 serial dilution, several single cell clones were isolated and verified for homozygous deletion by
158 PCR screening. PCR genotyping indicated successful homozygous deletion of the promoter or
159 YY1-binding motifs, respectively (Fig. 2B).

160 Loss of lnc-FANCI-2 expression in the single-cell clones was examined by RT-qPCR
161 (Fig. 2C). When compared to all control clones transfected and selected from an empty vector
162 containing no gRNA, all single cell clones with deletion of YY1-binding motifs (ΔYY1) showed
163 70-80% reduction of lnc-FANCI-2 expression, whereas the single cell clones with deletion of
164 both TSS1 and TSS2 promoters (ΔPr) showed >90% reduction (Fig. 2C). Northern blot analysis
165 confirmed the decrease in levels of the two major lnc-FANCI-2 isoforms (Fig. 2D), with an
166 abundant 4-kb lnc-FANCI-2 RNA derived from a distal polyadenylation site pA2 and a less
167 abundant 2-kb of lnc-FANCI-2 RNA derived from a proximal polyadenylation site pA1[8] (Fig.
168 2A and 2D). Reduced lnc-FANCI-2 RNA expression was also confirmed by RNAscope RNA-
169 ISH (Fig. 2E and 2F). The parental (WT) CaSki cells expressed ~10 copies of lnc-FANCI-2

170 RNA per cell [8], whereas the copy number of lnc-FANCI-2 RNA in the ΔYY1-D5 cells
171 dropped to ~5 copies and to ~2 copies per cell in the ΔPr-A9 cells (each averaged from 200
172 cells).

173 Although the WT CaSki cells preferentially grow as distinct cluster cell islands, the lnc-
174 FANCI-2 KO cells displayed a dispersed cell growth pattern and some cells exhibited an
175 irregular or spindle-like cell morphology (Fig. S2). The KO cells also grew slower than the
176 parental CaSki cells (Fig. 1G), formed fewer colonies with reduced size (Fig. 1H), and showed
177 decreased migration capacities (Fig. 1I), with ΔPr-A9 cells having a more severe phenotype than
178 ΔYY1-D5 cells. Subsequently, the ΔPr-A9 and ΔPr-B3 cells were further examined for their
179 HPV16 E6 and E7 expression and the ΔPr-A9 for cell senescence. We found both ΔPr-A9 and
180 ΔPr-B3 cells, when compared with parental WT CaSki cells, exhibited some small, variable
181 changes in the expression of E6, E7, p53 (E6 downstream target) and E2F1 (E7 downstream
182 target) proteins (Fig. S3A), most likely from sampling in the assays, but the ΔPr-A9 cells
183 displayed significant increase in cell senescence (Fig. S3B). Altogether, the data indicate that
184 lnc-FANCI-2 RNA is important for cell growth, colony formation, and cell migration.

185 **lnc-FANCI-2 regulates the expression and secretion of cell soluble receptors**

186 Considering that the altered expression of cell membrane proteins and secreted factors in
187 the lnc-FANCI-2 KO cells might contribute to the observed different cell morphology and
188 growth properties, we performed a Proteome Profiler Human sReceptor Array analysis to
189 examine possible changes in expression of 105 well-characterized soluble protein receptors
190 being involved in cell signaling using total cell lysates and cell culture supernatants from ΔPr-A9
191 and WT CaSki cells.

192 Using 30% cut-off (FC -/+0.3), we identified from the ΔPr-A9 cell lysate nine proteins
193 with increased expression compared to the WT CaSki cells, including PODXL2, ECM1,
194 NECTIN2, MCAM, ADAM9, ADAM10, CDH5, ITGA5 and NOTCH1, and six proteins with
195 decreased expression including ITGB6, CDH13, LGALS3BP, TIMP2, ADAM8 and SCARF2
196 (Fig. 3A and 3B). We also found from the ΔPr-A9 cell culture supernatant five proteins with
197 increased expression, including ADAM9, NECTIN2, ADAM10, CDH5 and ECM1, and the
198 decreased expression of four proteins, including CRELD2, SDC1, SDC4 and TIMP2 (Fig. 3A
199 and 3B). By immunoblot assays, we verified selectively the increase in PODXL2, MCAM, and
200 ECM1 and the decrease in ADAM8 and TIMP2 from the ΔPr-A9 cell lysates and the increase in
201 ECM1 and the decrease in TIMP2 in the ΔPr-A9 cell culture supernatant (Fig. 3C). As ADAM8
202 is proteolytically processed into two protein isoforms for cell adhesion [43] and migration[44],
203 we confirmed by immunoblot the decreased expression of all three sizes of ADAM8 protein in
204 the ΔPr-A9 cell lysate over the WT CaSki cells (Fig. 3C).

205 **lnc-FANCI-2 regulates the expression of genes involved in RAS signaling**

206 We next conducted genome-wide RNA-seq analyses of WT and lnc-FANCI-2 KO cells
207 (four samples/group) to determine the transcriptomic consequences of lnc-FANCI-2 deficiency.
208 We obtained ~120 million mappable RNA reads to the human reference genome hg38 from each
209 sample. Analysis of RNA-seq reads-coverage map by Integrative Genomics Viewer (IGV)
210 showed ~90% reduction of lnc-FANCI-2 expression in ΔPr-A9 cells and ~72% decrease in
211 ΔYY1-D5 cells compared to the WT CaSki cells (Fig. 4A), consistent with the results shown in
212 Fig. 2C-F.

213 Hierarchical clustering analysis showed more global transcriptional similarity between
214 ΔYY1-D5 and ΔPr-A9 cells (Fig. 4B). By applying a threshold of fold change (FC) ≥ 1.8 or FC

215 ≤ -1.8 with FDR ≤ 0.01, we found 1230 genes in ΔPr-A9 and 797 genes in ΔYY1-D5 cells with
216 significantly differential expression relative to the WT CaSki cells expressing ~15890 genes.
217 Nine (*Italic*) of 15 (60%) soluble receptor proteins in cell lysates (PODXL2, ECM1, *NECTIN2,*
218 *MCAM, ADAM9*, CDH5, ADAM10, *ITGA5*, *NOTCH1*, SCARF2, ADAM8, *TIMP2*, *LGALS3BP*,
219 *CDH13*, and *ITGB6*) exhibited consistent changes in expression by both RNA-seq and protein
220 array assays. The most significantly affected genes are shown in Volcano plots (Fig. 4C and
221 Table S1). Among these, 211 were upregulated and 189 were downregulated in both ΔPr-A9 and
222 Δ YY1-D5 cells (Fig. 4D and Table S2). By applying more stringent criteria with FPKM ≥7 in at
223 least one of four RNA-seq samples as a cutoff, we profiled the genes with large expression
224 differences in both ΔPr-A9 and ΔYY1-D5 cells. The results displayed in the heatmap of Fig. 4E
225 included 52 upregulated, and 47 downregulated genes excluding lnc-FANCI-2. Subsequently, we
226 selectively verified by RT-PCR the decreased expression of ITGB6, NLRP2, PLAC8, PSG4,
227 PSMB9, and SERPINB1 and the increased expression of CFH, CNTN5, EMP3, IGFBP3,
228 PTGS2, and SERPINB2 in ΔPr-A9 cells (Fig. 4F), as well as the increased expression of
229 IGFBP3 protein, a RAS signaling driver [30-32], in ΔPr-A9 cells by immunoblot (Fig. 4G).

230 By performing the Gene Set Enrichment Analysis (GSEA) on the Hallmark gene sets,
231 which provide more refined and concise inputs for GSEA [45], we found the most significantly
232 upregulated pathways in both ΔPr-A9 and ΔYY1-D5 cells, when compared with the WT CaSki
233 cells, were KRAS signaling and epithelial mesenchymal transition (EMT). The most
234 significantly downregulated pathways in both ΔPr-A9 and ΔYY1-D5 cells over the WT CaSki
235 cells were interferon gamma (IFN-γ) and interferon alpha (IFN-α) responses (Fig. 5A). GSEA
236 plots for ΔPr-A9 shows 29 of 111 genes, including IGFBP3 [30-32], in RAS signaling and 39 of
237 130 genes in EMT (Fig. 5B and 5C, Table S3) were significantly upregulated, whereas 37 of 139

genes in IFN-γ response and 24 of 71 genes in IFN-α response were significantly downregulated (Fig. 5D and 5E, Table S3). Similar enriched gene sets with increased RAS signaling and EMT and decreased IFN-γ and IFN-α responses were observed in ΔYY1-D5 cells (Fig. S4, Table S3).

Since ΔPr-A9 cells exhibit higher KO efficiency of lnc-FANCI-2 and a higher number of differentially expressed genes (DEGs) and show more severe phenotypic changes in cell proliferation, migration, and colony formation than ΔYY1-D5 cells, the ΔPr-A9 cells were primarily used for further focused studies on RAS signaling in this report.

lnc-FANCI-2 regulates RAS GTPase activities to phosphorylate RAS signaling effectors Akt and Erk

RAS activation triggers two major downstream signal transduction pathways, Raf/Mek/Erk and PI3K/Akt (Fig. S5), to transduce signals from extracellular stimuli to the cell nucleus where specific effector genes are activated for their corresponding functions [30-32, 46, 47]. To further confirm the GSEA data and verify that two major signaling pathways of RAS are activated, we first examined and compared the RAS GTPase activities in ΔPr-A9 cells and the WT CaSki cells. We found a significant increase in RAS GTPase activity in ΔPr-A9 cells (Fig. 6A, top bar graphs), indicating that the endogenous lnc-FANCI-2 RNA in CaSki cells suppresses not only the expression of IGFBP3 (Fig. 4F and 4G), the most abundant IGFBP, but also RAS activation (Fig. 6A, top bar graphs). Since ΔPr-A9 cells had undergone long term selection and adaption during single cell screening, the increased RAS GTPase activity might result from selection pressure for cell survival. However, by transient siRNA knockdown (KD) of lnc-FANCI-2 expression in the WT CaSki cells, we obtained a similar, albeit weaker, increase of RAS GTPase activity (Fig. 6A, lower bar graphs). This result suggests that the increased RAS

260 GTPase activity in ΔPr-A9 cells was unrelated to the persistent selection pressure, but rather the
261 deficiency of lnc-FANCI-2.

262 Next, we examined activation of the PI3K/Akt and Raf/Mek/Erk pathways [48-50]. We
263 observed a 3-fold increase in phosphorylated Akt (p-Akt) and 2.5-fold increase of p-Erk1/2
264 (p44/p42 MAPK), after being normalized to total Akt and Erk levels, in ΔPr-A9 cells over the
265 WT CaSki cells (Fig. 6B). These results were confirmed in ΔYY1-D5 cells (Fig. S6A). The
266 increased p-Akt and p-Erk (mostly p-Erk2/p42) was accompanied by elevated expression of
267 MCAM, VIM, and CCND2, and decreased expression of RAC3 (Fig. 6B and Fig. S6A). These
268 randomly chosen potential RAS effector proteins facilitate soluble receptor functions, cell
269 proliferation, and EMT. Moreover, transient siRNA knockdown of lnc-FANCI-2 in the WT
270 CaSki cells also led to the increased levels of p-Akt and p-Erk (Fig. 6C) and increased
271 expression of MCAM and VIM at 48 h and 96 h post-transfection (Fig. 6C). These observations
272 indicate that a transient loss of lnc-FANCI-2 in CaSki cells is sufficient to trigger RAS signaling.
273 The same siRNA transfection in HeLa cells, a lnc-FANCI-2 negative cell line (Fig. S1A and
274 S1B), exhibited no effect on p-Akt or p-Erk1/2 levels (Fig. S6B), but in SiHa cells containing
275 mainly nuclear lnc-FANCI-2 (Fig. S1C and S1D) enhanced the expression of p-Akt and p-Erk1/2
276 (Fig. S6B), verifying the specific effect of lnc-FANCI-2 depletion on RAS signaling pathways
277 independently of predominant cellular distribution of lnc-FANCI-2. The lnc-FANCI-2 KO-
278 mediated increase in p-Akt and p-Erk was sensitive to PI3K inhibitor LY294002 [51] (Fig. 6D,
279 lanes 4-6) and MEK1/2 inhibitor U0126 [52] (Fig. 6D, lanes 7-9), respectively. The inhibitors
280 also decreased the expression of VIM and MCAM and cell proliferation, in particular by
281 MEK1/2 inhibitor U0126 (Fig. 6D and 6E). The effects of LY294002 on cell proliferation were
282 similar from ΔPr-A9 to the WT CaSki cells (Fig. 6E).

283 **lnc-FANCI-2 inhibits the expression of IGFBP3 and MCAM (CD146 or MUC18)**

284 Given that IGFBP-3 is the most abundant IGFBP among all six IGFBP members in
285 potentiation of IGF action and PI3K/AKT activities [30] and a reduced expression of IGFBP-3
286 mRNA level is associated with progression to cervical cancer [53], we further investigated the
287 effect of lnc-FANCI-2 on the expression of IGFBP3 as lnc-FANCI-2 effector gene. As shown in
288 Fig. 4F-G and Fig. S7A, the increased RNA and protein expression of IGFBP3 appears in the
289 lnc-FANCI-2 KO ΔPr-A9 cells over the parental WT CaSki cells, indicating a suppressive effect
290 of lnc-FANCI-2 on IGFBP3 expression. This suppressive function of lnc-FANCI-2 was further
291 confirmed in lnc-FANCI-2 rescue experiments in the ΔPr-A9 cells (Fig. 7A and 7B). By
292 transient expression of one major isoform of lnc-FANCI-2 RNA (a-PA2, GenBank:
293 MT669800.1) [8] in the ΔPr-A9 cells, lnc-FANCI-2 (red) and IGFBP3 RNA (green) at 24 h post
294 transfection were detected by RNAscope RNA-ISH using each specific antisense RNA probe
295 (Fig. 7A). We demonstrated that the cells with rescued expression of cytoplasmic lnc-FANCI-2
296 RNA displayed much reduced expression of cytoplasmic IGFBP3 RNA (Fig. 7B).

297 As shown in Fig. 4E and Fig. S7B, the increased RNA expression of MCAM (CD146 or
298 MUC18) [54] appears to be transcriptional or posttranscriptional in both ΔPr-A9 and ΔYY1-D5
299 cells. We confirmed by RT-PCR the lnc-FANCI-2 KO-mediated increase of MCAM RNA
300 expression in ΔPr-A9 cells (Fig. 7C). A rescue experiment was further performed by transient
301 expression of one major isoform of lnc-FANCI-2 RNA (a-PA2, GenBank: MT669800.1) [8] in
302 ΔPr-A9 cells to determine both nuclear and cytoplasmic MCAM expression [55, 56] in
303 individual lnc-FANCI-2 expressing cells. ΔPr-A9 cells ectopically expressing diffused
304 cytoplasmic lnc-FANCI-2 RNA, as detected by RNAscope RNA-ISH, exhibited a marked
305 reduction in nuclear MCAM protein (Fig. 7D-7E). Quantitative analyses of the ΔPr-A9 cells with

306 or without transient lnc-FANCI-2 RNA expression showed significant reduction of nuclear
307 MCAM protein in the 35 cells with rescued lnc-FANCI-2 expression when compared to the 54
308 cells expressing no lnc-FANCI-2 (Fig. 7F). Due to RNAscope procedures, the membrane-bound
309 and cytoplasmic MCAM protein was mostly removed by protease III treatment when RNA-ISH
310 was performed and thus only the nuclear signal of MCAM protein remained was detectable by IF
311 staining. Using cell fractionation, we detected a cleaved MCAM of ~46 kDa mainly in the
312 nuclear fraction by Western blot (Fig. 7G). The increased nuclear MCAM expression in ΔPr-A9
313 cells was proportional to the cytoplasmic and total MCAM levels when compared with the WT
314 CaSki cells (Fig. 7G). The nuclear MCAM signal appeared as a proteolytic cleavage product
315 presumably by the increased metalloprotease ADAM9 and ADAM10 proteins and decreased
316 metalloprotease inhibitor TIMP2 (Fig. 3), as observed in other studies [56].

317 The significance of an inverse correlation of lnc-FANCI-2 and MCAM in CaSki cells
318 was further investigated by analyzing their expression in 304 cervical cancer samples from the
319 TCGA dataset. There was a significant negative correlation in lnc-FANCI-2 (being wrongly
320 assigned as LINC00925 by NCBI) [8] and MCAM RNA levels (Fig. 7H). The opposite effects of
321 lnc-FANCI-2 and MCAM on cervical cancer survival (Fig. 7I and Fig. S8) show that the cervical
322 cancer patients with a higher level of lnc-FANCI-2 [8] but a lower level of MCAM in the
323 cervical tissue (Fig. S8 and Fig. 7I) exhibited a better survival prognosis.

324 **Regulatory roles of lnc-FANCI-2-mediated increase of MCAM and IGFBP3 on RAS**
325 **signaling**

326 To further dissect the lnc-FANCI-2-associated expression of MCAM and IGFBP3 on
327 RAS signaling, we examined MCAM and IGFBP3 on phosphorylation of Akt and Erk1/Erk2 in
328 CaSki cells in the presence or absence of lnc-FANCI-2. As shown in Figure 7J, we found,

329 although KD or KO of lnc-FANCI-2 promotes phosphorylation of Akt and Erk (Fig. 7J, lane 2),
330 that KD of MCAM expression in the parental WT CaSki cells in the absence of lnc-FANCI-2
331 (Fig. 7J, lane 3) or in ΔPr-A9 cells (Fig. 7J, lane 5) led to reduction of Akt and Erk
332 phosphorylation. These data suggest that MCAM is a lnc-FANCI-2 effector but also could be a
333 trigger of signal transduction as reported [54, 57].

334 IGFBP3 protein has been viewed as a RAS signaling regulator [30-32], but recent studies
335 show that IGFBP3 has a variety of intracellular ligands involved in many unexpected functions
336 [58, 59]. Thus, KD or KO of lnc-FANCI-2-mediated IGFBP3 expression on RAS signaling in
337 the parental WT CaSki cells or ΔPr-A9 cells was examined by Western blot after siRNA KD of
338 IGFBP3 expression. As shown in Figure 7K, KD of IGFBP3 expression was found to increase
339 phosphorylation of Erk1/2 by ~70% (lane 4) to ~60% (lane 6), but not much so for Akt
340 phosphorylation (lanes 4 and 6). Instead, KD of IGFBP3 expression could prevent lnc-FANCI-2
341 KD-enhanced Akt phosphorylation in the parental WT CaSki cells (Fig. 7K, compare lane 2 and
342 lane 3). These data suggest a separate role of IGFBP3 on phosphorylation of Erk1/2 from Akt in
343 the presence or absence of lnc-FANCI-2.

344 **MAP4K4 association with lnc-FANCI-2 RNA in CaSki cells regulates RAS signaling and**
345 **phosphorylation of Akt and Erk**

346 We speculated lnc-FANCI-2 restriction on RAS signaling through interactions with
347 cellular proteins. Subsequently, comprehensive identification of lnc-FANCI-2-binding proteins
348 in the parental WT CaSki cells was performed by an IRPCRP protocol (modified from published
349 ChIRP [60]) in combination with mass spectrometry (Fig. 8A). In this protocol, the lnc-FANCI-
350 2-binding proteins in the parental WT CaSki cells were covalently crosslinked to lnc-FANCI-2
351 RNA via UV irradiation and pulled down by pooled 30 antisense oligos crossing over the entire

352 lnc-FANCI-2. The RNA extracted from the pulldowns were verified to be lnc-FANCI-2 specific
353 by RT-PCR in the absence (-) or presence (+) of reverse transcriptase (RT) (Fig. 8B). The lnc-
354 FANCI-2-binding proteins in the pulldowns were then subjected to LC-MS/MS analyses. We
355 identified 32 specific lnc-FANCI-2-binding proteins, including H13, HNRH1, K1H1, MAP4K4,
356 and RNPS1 (Fig. 8C, Table S4).

357 MAP4K4, a serine/threonine protein kinase, stimulates cancer cell proliferation, invasion
358 and migration, and is recently characterized as a novel MAPK/ERK pathway regulator [61-63]
359 and negatively regulates RAS signaling by binding to Ras p21 protein activator 1 or RASA1
360 [64, 65]. Although the exact MAK4K4 binding site on lnc-FANCI-2 was not explored, many
361 enzymes turn out an RNA-binding enzyme [66, 67]. Thus, whether MAP4K4 association with
362 lnc-FANCI-2 could regulate PI3K/Akt or MAPK/Erk signal transduction was investigated in the
363 parental WT CaSki cells. We demonstrated that siRNA KD of MAP4K4 expression in the
364 parental WT CaSki cells, as seen for KD of lnc-FANCI-2, led to ~40% or more increase of
365 phosphorylation of both Akt and Erk1/2 and increased expression of MCAM and IGFBP3 (Fig.
366 8D, compare lane 2 to lane 3). Interestingly, siRNA KD of MAP4K4 expression in the lnc-
367 FANCI-2 KO ΔPr-A9 cells had no effect on expression of IGFBP3, only a minimal effect on
368 MCAM, but strongly on pErk1/2 (Fig. S7C). The data suggest that, through RNA-protein
369 interactions, the increased lnc-FANCI-2 RNA in cells and their association with MAP4K4 and
370 other cellular proteins could be one arm to control RAS signaling and gene expression of its
371 effectors (Fig. 8E).

372

373

374 **DISCUSSION**

375 HPV oncoproteins E6 and E7 are necessary but not sufficient for development of cervical
376 cancer. Indeed, early studies indicated that other oncogenic stress, such as activated RAS mutant,
377 is needed to trigger malignant transformation of E6 and E7 expressing cells [21, 26, 68, 69] and
378 tumorigenesis [27, 28, 70-74]. Moreover, E7 has been also reported to repress phosphorylation
379 of Akt and Akt-mediated signaling [75]. In this study, we show that lnc-FANCI-2, whose
380 expression is highly dependent on E7 and YY1 [8], intrinsically restricts RAS GTPase activities
381 and phosphorylation of Akt and Erk presumably by interacting with cellular factors in HPV16-
382 positive CaSki cells. Interestingly, early reports indicated that p-Akt attenuation by E7 could be
383 abolished by introduction of H73E mutation in the E7 CR3 domain [75]. This E7 CR3 domain is
384 also essential to interact with transcription factor YY1 to activate lnc-FANCI-2 transcription [8].
385 Thus, it would be presumable that the reported p-Akt attenuation by E7 might be mediated by the
386 increased expression of lnc-FANCI-2. More importantly, these findings also suggest that
387 additional oncogenic stress, such as activated RAS mutant, is required to overcome the lnc-
388 FANCI-2 restriction on RAS signaling for the early observed malignant transformation [21, 26,
389 68, 69] and tumorigenesis [27, 28, 70-74] of E6 and E7 expressing cells. In CaSki cells, loss of
390 lnc-FANCI-2 in this report was found to promote RAS signaling but reduction of IFN responses.
391 However, high RAS-AKT-ERK signaling induces cell senescence and inhibits tumor cell
392 survival as shown in this report and in a lung cancer study [76].

393 Some lncRNAs function as RAS regulators [77, 78] by their ability to sequester RAS-
394 targeting miRNAs, including MALAT1/ miR-217, RMRP/miR-206, and KRAS1P/miR-143/let-
395 7 [78]. Conceivably, lncRNAs may also regulate RAS signaling through other mechanisms
396 beyond miRNAs. In this report, loss of lnc-FANCI-2 in HPV16-positive CaSki and SiHa cells

397 promotes RAS signaling and expression of RAS signaling effectors (Fig. 8E). By profiling the
398 proteins associated with lnc-FANCI-2 in CaSki cells, we identified a serine/threonine protein
399 kinase MAP4K4 as one of major lnc-FANCI-2-binding proteins that may partially mediate the
400 lnc-FANCI-2 restriction on RAS signaling. MAP4K4 is a negative RAS signaling regulator in
401 the context of the early embryo [62, 64] and lymphatic vascular development by interacting with
402 RASA1 [65]. Indeed, silencing of MAP4K4 in parental WT CaSki cells, like KD or KO of lnc-
403 FANCI-2, led to partially increase of both p-Akt and p-Erk1/2 (Fig. 8D) as reported [64, 65].
404 Interestingly, KD of MAP4K4 in ΔPr-A9 cells led to further increased expression of p-Erk1/2
405 but not p-Akt, suggesting a negative correlation of MAP4K4 activity in interaction with lnc-
406 FANCI-2 on Erk1/2 phosphorylation. Thus, our data suggest that MAP4K4 protein may
407 function coordinately with lnc-FANCI-2 RNA in the CaSki cells to restrict one arm but not the
408 other of RAS signaling.

409 All HR-HPVs are capable of inducing lnc-FANCI-2 expression by experimental infection
410 of keratinocytes [8]. HPV^{+} cervical cancer tissues express high level of lnc-FANCI-2. As
411 expected, all HPV16^{+} cervical cancer and pre-cancer cell lines examined, such as CaSki, SiHa,
412 W12 subclone cells 20861(HPV16^{+}, integrated) and 20863 (HPV16^{+}, episomal), produce lnc-
413 FANCI-2. Unexpectedly, we found no expression of lnc-FANCI-2 in isogenic HPV18^{+} HeLa
414 and C4II cells, nor in colorectal cancer cell line HCT116, adenovirus 5 DNA-transformed human
415 embryonic kidney cell line HEK293, spontaneously transformed aneuploid immortal
416 keratinocyte cell line HaCaT, and KSHV-infected B cell lymphoma cell line BCBL-1 cells
417 which are all HPV-negative cell lines. It remains to know what negatively regulates lnc-FANCI-
418 2 expression in those cell lines and more HPV18^{+} cell lines should be examined for lnc-FANCI-
419 2 expression. However, we did find that a HPV-negative cervical cancer cell line, C33A cells

420 expressing mutant p53 and mutant pRB [41], produce a high level of lnc-FANCI-2 (Fig. S1A
421 and S1B). Using dual luciferase report assays, we did find lnc-FANCI-2 promoter activity in
422 response to YY1 binding in CaSki and C33A cells, but not in HeLa and HCT116 cells,
423 suggesting the presence of a repressive factor (s) in the latter two cell lines (data not shown). KD
424 of E2F1 had no effect on lnc-FANCI-2 promoter activity in CaSki cells [8]. In the lnc-FANCI-2
425 producing cells, we noticed that cellular location of lnc-FANCI-2 also varies from cell types,
426 with lnc-FANCI-2 predominantly in the nucleus in SiHa and C33A cells, but in the cytoplasm in
427 CaSki cells, although both cytoplasmic and nuclear lnc-FANCI-2 restrict RAS signaling. This
428 suggests that a variety of nuclear and cytoplasmic functions of lnc-FANCI-2 remains to be
429 explored.

430 IGFBP3 is a major IGF carrier and enhances both IGF- and EGF-RAS signaling [31, 79]
431 to activate phosphatidylinositol 3-kinase (PI3K)/AKT and the mitogen-activated protein kinase
432 (MAPK)/ERK pathways [80]. Surprisingly, we find a suppressive role of IGFBP3 on Erk
433 phosphorylation, but not much on Akt, in the presence or absence of lnc-FANCI-2 in HPV16-
434 positive CaSki cells. Although ~99% of circulating IGF-1 is bound to IGFBPs, predominantly to
435 IGFBP-3, the most abundant IGFBP in human serum, case-control studies showed significantly
436 lower IGF-1 and IGFBP-3 serum levels in the patients with invasive cervical cancer over the
437 control group [81, 82]. A reduced expression of IGFBP-3 mRNA level appears to be associated
438 with progression to cervical cancer [53]. Consistently with lnc-FANCI-2's suppressive effect on
439 IGFBP3 expression in our study, an increased level of lnc-FANCI-2 expression is associated
440 step-wisely with high-risk HPV-positive cervical intraepithelial neoplasia and invasive cervical
441 cancer tissues [8].

442 It is obvious from our RNA-seq and human soluble receptor array analysis that KO of
443 lnc-FANCI-2 in CaSki cells affects the expression of a large set of genes, including the
444 expression of increased NECTIN2, ADAM9, ADAM10, ITGA5, MCAM, PODXL2, ECM1, but
445 decreased ADAM8, TIM2, and ITGB6, which are responsible for RAS signaling, EMT pathway,
446 and IFN responses. For example, the dysregulation of RAS signaling and ADAM protein activity
447 is implicated in various cancers. ADAM proteins can modulate RAS signaling by cleaving and
448 releasing ligands that activate or inactivate RAS-related pathways [83-86]. Some ADAM
449 proteins are Involved in the migration and invasion of cancer cells, and its loss can promote the
450 degradation of KRAS [87]. ADAMs are essential for extracellular signaling and regulation of
451 cell adhesion and their catalytic activity is strongly correlated to Src-homology 3 (SH3) domain
452 binding of SH3 proteins [85, 86, 88]. In addition to the notified activation of PI3K/Akt and
453 Raf/Mek/Erk pathways, one of the major RAS signaling effectors in lnc-FANCI-2 KO or KD
454 cells was found to be MCAM.

455 MCAM binds various cellular surface receptors or co-receptors to trigger signal
456 transduction, cell proliferation and motility, tumor angiogenesis, and tumor cell metastasis [54,
457 57]. It is an integral, highly glycosylated membrane protein with three common protein isoforms
458 [54, 89, 90]. Two membrane-anchored forms with a long (p113) or short (p76) cytoplasmic tail
459 produced by alternative RNA splicing and a proteolytically cleaved soluble form without
460 transmembrane and cytoplasmic regions [54, 90, 91]. In addition to its roles in cell signal
461 transduction [54, 57, 89, 90], the short isoform produced by an intramembrane cleavage may be
462 directed towards the nucleus to regulate gene transcription [56]. We found that CaSki cells
463 express mainly a cytoplasmic form of full-length MCAM (~113 kDa) and a small nuclear form
464 (~46 kDa), but not the short ~76 kDa isoform. Moreover, lnc-FANCI-2 KO cells exhibit high

465 MCAM levels, which was most likely a result of the increased RAS signaling. Consistently, lnc-
466 FANCI-2 and MCAM levels are negatively correlated in cervical cancer patients, and low levels
467 of MCAM and high levels of lnc-FANCI-2 indicate better prognosis. This suggests that
468 increased MCAM might promote cervical tumorigenesis in vivo. Given that the cells with lnc-
469 FANCI-2 KO exhibit increased levels of IGFBP3 and MCAM and the ΔPr-A9 cells with rescued
470 lnc-FANCI-2 RNA expression displayed remarkable reduction of IGFBP3 and MCAM
471 expression, our current model (Fig. 8E) highlights how the HPV16-enhanced expression of lnc-
472 FANCI-2 in cervical cancer cells might function as a negative regulator by binding to various
473 RNA-binding proteins to block RAS signaling and reduce the expression of RAS signaling
474 effectors such as IGFBP3 and MCAM, etc.

475 In conclusion, this study provides the first evidence that one of lnc-FANCI-2 functions is
476 to maintain epithelial functional integrity by repressing RAS signaling in preventing malignant
477 transformation of neoplastic cervical lesions. In addition, more extensive studies are undergoing
478 to elucidate the role of lnc-FANCI-2 in regulation of IFN responses, which are not covered in
479 this report. Since transactivation of lnc-FANCI-2 expression is largely dependent on host
480 transcription factor YY1 of which expression is regulated by HPV oncoproteins and host miR-
481 29a, dissecting their transcription network on lnc-FANCI-2 and its effectors may further provide
482 novel insights involved in host homeostasis against HPV infection-induced carcinogenesis. Our
483 observations also highlight additional, unexpected players beyond viral E6 and E7 that drive
484 cells toward malignant transformation.

485 **MATERIALS AND METHODS**

486 **Cell cultures and treatment**

487 CaSki, a HPV16-positive (HPV16$^+$) human cervical cancer cell line with wild-type p53, pRb,
488 HRAS, KRAS, and NRAS (https://depmap.org/portal/cell_line/ACH-001336?tab=mutation) was
489 obtained from the American Type Culture Collection (ATCC, Manassas, VA), maintained in
490 Dulbecco's modified Eagle medium (DMEM) (Thermo Fisher Scientific) supplemented with
491 10% fetal bovine serum (FBS) and 1% penicillin-streptomycin, and grown in a cell culture
492 incubator at 37°C with 5% CO_2.

493 SiHa (HPV16$^+$), HeLa (HPV18$^+$), C4II (HPV18$^+$), C33A (no HPV), and other HPV-
494 negative cell lines, HEK293T (Ad5 E1/E2-immortalized human kidney cells), and HaCaT
495 (spontaneously immortalized human epidermal cells), were all obtained from ATCC and grown
496 in Dulbecco's modified Eagle's medium (DMEM) with 10% FBS at 37°C and 5% CO_2. HCT116
497 cell line, a colorectal cancer cell line, was a gift from Dr. Bert Vogelstein of Johns Hopkins
498 University and was grown in McCoy's 5A medium with 10% FBS at 37°C and in 5% CO_2. W12
499 subclones 20861 (HPV16$^+$, integrated) and 20863 (HPV16$^+$, episomal) were a gift from Dr. Paul
500 Lambert of University of Wisconsin, Madison, and grown on mitomycin C-pretreated NIH3T3
501 feeder cells in F12 medium at 37°C and in 5% CO_2. BCBL-1 (body cavity B lymphoma cells
502 with KSHV infection) was obtained from the AIDS Research and Reference Reagent Program,
503 Division of AIDS, NIAID, NIH and cultured in RPMI 1640 containing 10% FBS at 37°C and in
504 5% CO_2.

505 CaSki cells were treated with 20 μM phosphoinositide 3-kinase (PI3K) inhibitor,
506 LY294002 (Cell Signaling Technology, Danvers, MA, #9901) or 10 μM mitogen-activated
507 protein kinase kinase (MEK) inhibitor, U0126 (Cell Signaling Technology, Danvers, MA,
508 #9903) and examined for their proliferation and viability by CCK-8 assay and RAS effector
509 expression by Western blot.

510 **Raft tissues and cervical tissue sections**

511 Raft tissues with or without HPV16 or HPV18 infection and cervical cancer tissue sections from
512 Zhejiang University Women's hospital were described in our previous reports [8, 92].

513 **siRNAs, plasmid constructions and transfections**

514 Synthetic double-stranded siRNA targeting the lnc-FANCI-2 transcript is listed in a
515 supplementary Table S5. Human MAP4K4 siRNA (#M-003971), human IGFBP3 siRNA (#M-
516 004777) and non-targeting control siRNA(#D-001210-01) were purchased from Dharmacon, Inc
517 (Lafayette, CO). Each siRNA transfection into CaSki or other type of cells was carried out by
518 LipoJet in vitro transfection reagent (SignaGen, Frederick, MD, USA). Plasmid pHBL03 has a
519 short isoform of lnc-FANCI-2 cDNA (lnc-FANCI-2a-PA1, GenBank Acc. No. MT669801).
520 Overlapping PCR products generated from 5' and 3' RACE PCR products with a primer pair of
521 oHBL 17 and oHBL 18 were digested and inserted into pcDNA3 at Hind III and Xba I sites. The
522 insertion was verified by sequencing. Plasmid pHBL05 has a long isoform of lnc-FANCI-2 (lnc-
523 FANCI-2a-PA2, GenBank Acc. No. MT669800). PCR products generated from genomic DNA
524 with oHBL 19 and oHBL 23 were digested and swapped into pHBL03 to replace lnc-FANCI-2a-
525 PA1 at Bsmb I and Xba I sites.

526 CRISPR/Cas9 system was used to knockout lnc-FANCI-2 gene from CaSki cells. Two
527 lnc-FANCI-2 specific guide RNAs (gRNAs) were designed by an on-line CRISPR design tool
528 developed by the Zhang lab (http://crispr.mit.edu). A modified cloning strategy was used to
529 clone the two gRNA into pSpCas9(BB)-2A-Puro vector (Addgene, Watertown, MA, #62988)
530 and described in our previous publication [42]. This strategy allows all three components (two
531 gRNAs and Cas9) express from the same plasmid to ensure the transfected cells expressing two

532 gRNAs simultaneously knocking out the targeted gene [42]. The sequences of primers to make
533 guide RNAs were listed in Supplementary Table S5.

534 **Knockout of lnc-FANCI-2 gene in CaSki cells, PCR screening and genotyping**

535 Two gRNAs each under control by a U6 promoter in a pSpCas9(BB)-2A-Puro vector were used
536 to create deletion in CaSki cells. Plasmid pHBL25 which contains gRNA 1 and 6 was used to
537 delete the entire promoter region of lnc-FANCI-2 and plasmid pHBL27 which contains gRNA 3
538 and 4 was used to delete only two YY1-binding motifs spanning over an 87-bp region in the lnc-
539 FANCI-2 promoter. CaSki cells transfected with the gRNA-expressing vectors were then under 2
540 weeks of puromycin selection (0.1 μg/ml). The puromycin-resistant CaSki cells were diluted to a
541 final concentration of 0.5 cells per 100 μl, plated 100 μl of diluted cells into each well of a 96-
542 well plate, and grew under continuous purymycin selection. The colonies were inspected to
543 ensure the clones were grown from one cell, and refed or re-plated as needed in 3 weeks of
544 expansion.

545 A direct PCR was performed for number of single cell clones as described [42]. Briefly,
546 several hundreds of cells expanded from a single cell clone were resuspended in 50 μl of
547 phosphate-buffered saline (PBS) and then frozen-thawed on dry ice for three times. Cell lysates
548 were treated with 4 μl of Qiagen protease (QIAGEN, Hilden, Germany, #1017782,) at 56°C for
549 10 min, and the protease was inactivated at 95°C for 5 mins. The resulting product was directly
550 used for PCR screening. P1 + P5 were used for verification of promoter deletion and P3 + P4 for
551 YY1 motifs deletion. To ensure the selected single cell clones displaying homozygous knockout
552 of lnc-FANCI-2, total cell DNA was isolated using a QIAamp DNA Blood Minikit (QIAGEN,
553 Hilden, Germany, #51106) and then the homozygous deletion was screened and the cells with
554 homozygous KO were selected and confirmed by PCR. The primers used for genotyping are

555 listed in supplementary Table S5. At least two single cell clones either with lnc-FANCI-2
556 promoter deletion or with YY1 motif deletion were selected. Three single cell clones from the
557 cells transfected with an empty vector, pSpCas9(BB)-2A-Puro, were also selected and served as
558 controls for the genotyping screening.

559 **Cell proliferation and viability assay**

560 Cell proliferation and viability were determined by a CCK-8 assay (Dojindo Molecular
561 Technologies, Rockville, MD). For proliferation assay, 500 µl of cell suspension (50,000
562 cells/well) were dispensed into individual wells in a 24-well plate. Cells were then treated with
563 inhibitors (20 µM LY294002, or 10 µM U0126 respectively) after 24 h culture. At each time
564 point of 24 h, 48 h and 72 h, 50 µl of CCK-8 solution was added in three wells of each group and
565 incubated for 1 h in a cell culture incubator at 37°C. Cell proliferation was determined by
566 absorbance at 450 nm, and normal medium was used to subtract background. Percentage of cell
567 viability was calculated by the following formula: cell viability % = OD450 of inhibitors treated
568 sample / OD450 of untreated sample × 100%.

569 **Colony formation, cell migration assay and senescence analysis**

570 CaSki Cells were seeded at 1×10^4, 5×10^3 or 1×10^3 cells/well in 6-well plates. After 24 h of
571 cell growth, the culture medium in each well was replaced by DMEM containing 1%
572 methylcellulose and 10% FBS. The plates were fixed with 3.7% formaldehyde and stained with
573 1% crystal violet in 2 weeks. Transwell cell migration assay was performed as previously
574 described [93]. Briefly, CaSki cells were re-suspended in serum free DMEM containing 0.1%
575 BSA. 1×10^5 cells in 100 ul were then plated on top of the filter membrane in a transwell insert
576 (SARSTEDT, Nümbrecht, GERMANY, # 83.3932.800) and incubate for 10 min at 37 °C to

577 allow the cells to settle down, then 600 µl of complete media containing 10% FBS were added
578 into the bottom of the lower chamber in a 24-well plate. After 24 h in culture, the cells on the top
579 of the insert membrane were removed, and cells on the bottom were fixed, stained by 0.2%
580 crystal violet and then counted.

581 Cell senescence was determined by Cellular Senescence Assay (MilliporeSigma,
582 Burlington, MA, # QIA117-1KIT). Briefly, CaSki Cells were plated at 2×10^5 cells/well in 6-
583 well plates and cultured for 2 days to 50% confluence. Cells were washed once with 2 ml PBS
584 and fixed with 0.5 ml of Fixative Solution at room temperature for 10 to 15 min. Then, cells
585 were washed twice with 2 ml PBS, and 1 ml Staining Solution was added to each well. Cells
586 were incubated at 37°C overnight without CO_2 and protected from the light. Blue stained cells
587 were then counted under light microscopy.

588 **Nuclear and cytoplasmic fractionation**

589 CaSki and SiHa cells were fractionated by using Nuclei EZ Prep Kit (Sigma-Aldrich, #NUC-
590 101) following the manufacturer's protocol. The details of the method could be found in our
591 previous publication [94]. Western blot analysis for nuclear protein SRSF3 and cytoplasmic
592 protein GAPDH was used to determine the fractionation efficiency. The fractionated cytoplasmic
593 and nuclear RNAs were used for detection of lnc-FANCI-2 RNA with human GAPDH RNA
594 serving as a control for RNA fractionation efficiency of the cytoplasmic RNAs.

595 **RT-qPCR**

596 Detection of lnc-FANCI-2 by RT-qPCR was performed as described [8]. Pre-designed primers
597 for lnc-FANCI-2 are listed in Table S5. Briefly, 2 µg total RNA was converted to cDNA using
598 Superscript First-stand Synthesis kit (Thermo Fisher Scientific, Waltham, MA, #11904018).

599 qPCR was performed using TaqMan gene expression Master Mix (Applied Biosystems,
600 Waltham, MA, #4369016) on a StepOne Plus Real-Time PCR system (Applied Biosystems).
601 TaqMan Gene Expression Assay (Applied Biosystems, #4331182) for GADPH
602 (Hs02758991_g1) was served as an internal control. Data were plotted as fold change over the
603 control group using the $2^{-\Delta\Delta Ct}$ method by which the data was normalized first to the values for
604 GAPDH and then to the median value for control samples. Data are presented as a bar graph with
605 mean ± SD for each group.

606 **Northern blot**

607 To validate lnc-FANCI-2 KO in CaSki cells, Northern blot was performed using polyA$^+$ mRNA
608 isolated from 100 µg of total CaSki RNA with PolyATtract mRNA Isolation Systems (Promega,
609 #Z5310) or 10 µg of total CaSki total RNA as described previously [8]. Briefly, RNA samples
610 were denatured in NorthernMax Formaldehyde loading dye (Thermo Fisher Scientific,
611 #AM8552) at 75°C for 15 min, then separated in an 1% formaldehyde-containing agarose gel
612 and transferred onto a GeneScreen Plus hybridization transfer membrane (Perkin Elmer,
613 Waltham, MA, #NEF987001PK). RNAs on the membrane were crosslinked by exposing to UV
614 light, and then prehybridized with PerfectHyb Plus hybridization buffer (Sigma-Aldrich, St.
615 Louis, MO, #H7003) for 2 h at 42°C. Specific oligos against lnc-FANCI-2 or GAPDH listed in
616 Table S5 were labeled with [γ-^{32}P]-ATP using T4 PNK (Thermo Fisher Scientific, Waltham,
617 MA, #18004–010) and added into hybridization buffer for overnight incubation at 42°C. The
618 membrane was then washed with 2× SSPE/0.5% SDS solution for 5 mins, followed by twice
619 washes with 0.5× SSPE/0.5% SDS each for 15 min at 42°C and then exposed to a
620 PhosphorImager screen.

621 **RNA-seq and data analysis**

622 Total RNA was from WT CaSki cells, ΔYY1-D5 and ΔPr-A9 cells were extracted using TRIzol
623 reagent (Thermo Fisher Scientific, Waltham, MA, #15596018). Total ribo-minus RNA-seq
624 libraries, four samples in each group, were prepared with TruSeq Stranded Total RNA Library
625 Kit and then subjected to pair-end sequencing using Illumina-HiSeq3000/4000 platform.

626 The obtained reads were processed using the CCBR Pipeliner utility
627 (https://github.com/CCBR/Pipeliner). Briefly, reads were trimmed from adapters and low-quality
628 bases using Cutadapt (version 1.18) (https://bioweb.pasteur.fr/packages/pack@cutadapt@1.18)
629 before alignment to the custom reference genome described below. The transcripts were aligned
630 using STAR v2.5.2b in two-pass mode [95]. Expression levels were quantified using RSEM
631 (RNA-Seq by Expectation-Maximization) (version 1.3.0) [96] with a custom gene annotation
632 described below.

633 The custom reference genome allowing quantification of both HPV16 and host
634 expression used in this alignment consisted of the human reference genome (hg38/Dec.
635 2013/GRCh38) with a HPV16 FASTA (https://pave.niaid.nih.gov/) sequence added as an
636 additional pseudochromosome. The custom gene annotation used for gene expression
637 quantification consisted of a concatenation of the hg38 GENCODE annotation version 30 [97]
638 and the HPV16 genome, with one other notable alteration. The hg38 v30 gene annotation is
639 incorrect at the location of the lnc-FANCI-2 locus in the hg38 genome at chr15:89378104-
640 89398487, which affects quantification of this gene. To correct this annotation and provide
641 accurate quantification, therefore, we first performed BLAST against hg38 using the sequences
642 of the 14 known isoform transcripts of lnc-FANCI-2 (MT669800 for lnc-FANCI-2a-PA2,
643 MT669801 for lnc-FANCI-2a-PA1, MT669802 for lnc-FANCI-2b-PA2, MT669803 for lnc-
644 FANCI-2b-PA1, MT669804 for lnc-FANCI-2c-PA2, MT669805 for lnc-FANCI-2c-PA1,

645 MT669806 for lnc-FANCI-2d-PA2, MT669807 for lnc-FANCI-2d-PA1, MT669808 for lnc-
646 FANCI-2e-PA2, MT669809 for lnc-FANCI-2e-PA1, MT669810 for lnc-FANCI-2f-PA2,
647 MT669811 for lnc-FANCI-2f-PA1, MT669812 for lnc-FANCI-2g-PA2, and MT669813 for lnc-
648 FANCI-2g-PA1). The results were used to determine the precise exon start and stop sites for
649 each of the isoforms. These were then used to manually adjust the default hg38 v30 gene
650 annotations at the locus indicated above to account for the correct structure of the lnc-FANCI-2
651 locus and its 14 isoforms.

652 Downstream analysis and visualization were performed within the NIH Integrated
653 Analysis Portal (NIDAP) using R programs developed on the Foundry platform (Palantir
654 Technologies). Briefly, raw counts data produced by RSEM were imported into the NIDAP
655 platform, genes were filtered for low counts (<1 cpm) and the voom algorithm [98] from the
656 Limma R package (version 3.40.6) [99] was used for quantile normalization and calculation of
657 differentially expressed genes. Pre-ranked GSEA was performed using the Molecular Signatures
658 Database version 6.2 [100, 101] and the fgsea package [102]. Raw data and the analyzed RNA-
659 seq data supporting the findings in this study have been deposited in the NCBI GEO database
660 (the accession#: GSE190904).

661 **Human Soluble Receptor Array**

662 To detect the changes of soluble receptors expressed and released from parental WT CaSki cells
663 and lnc-FANCI-2 KO cells, Proteome Profiler Human sReceptor (Soluble Receptor) Array
664 (R&D Systems, Minneapolis, MN, # ARY012) was performed according to a manufacturer
665 protocol. Briefly, 7×10^6 WT CaSki cells and ΔPr-A9 cells were cultured in 15 ml of DMEM
666 supplemented with 10% FBS in a T75 flask for 24 h. Cell culture supernatants were then
667 collected and centrifuged at 4,000 × g for 15 min to remove cell debris. Cells were rinsed by 10

668 ml of PBS and solubilized in Lysis Buffer 17 at 4°C for 30 min. The cell lysis was then
669 centrifuged at 14,000 × g for 5 min to remove cell debris. Protein concentration of cell lysis was
670 measured by Micro BCA Protein Assay (PIERCE, Waltham, MA, #23235). Next, two sets of N
671 and C membranes were blocking by Buffer 8/1 in 4-Well Multi-dish for 1 h on a rocking
672 platform. 500 µl of culture supernatant or 100 µg cell lysate generated from the WT CaSki cells
673 or ΔPr-A9 cells were diluted in 3 ml of Buffer 8/1 and then applied to each membrane after three
674 washes with 1× Wash Buffer. The membranes were incubated overnight at 4 °C on a rocking
675 platform and washed three times to remove unbound materials followed by incubation with their
676 specific cocktail of biotinylated detection antibodies for 2 h at room temperature on a rocking
677 platform. 2 ml of diluted Streptavidin-HRP was then applied to each membrane for 30 min at
678 room temperature on a rocking platform after three times of wash. 1 ml of the prepared Chemi
679 Reagent Mix was added onto the membranes after three times of wash. The signal was then
680 captured by ChemiDoc Touch Imaging System (Bio-Rad). Quantification of the relative protein
681 expression in ΔPr-A9 cells compared to the WT cells was determined in Image Lab software
682 (Bio-Rad). The average signal of duplicate spots subtracting background value from negative
683 control spots represented the levels of each protein. The relative change in protein levels was
684 then determined by comparing ΔPr-A9 cells to the WT cells.

685 **Antibodies and Immunoblot**

686 Immunoblot analysis was performed for individual proteins by using the following antibodies:
687 anti-MCAM (#17564-1-AP), anti-E2F1 (#12171-1-AP), anti-MAP4K4 (#55247-1-AP), and anti-
688 p53 (#10442-1-AP) antibodies were from ProteinTech (Rosemont, IL). Anti-tubulin (#T5201)
689 antibodies were from Sigma-Aldrich (St. Louis, MO). Anti-hnRNP C1/C2 (#Ab10294) and anti-
690 RAC3 (#ab129062) antibodies were from Abcam (Cambridge, United Kingdom). Anti- CCND2

691 (Cyclin D2, #3741), anti-Akt (#9272), anti-phospho-Akt (#9271), anti-Erk1/2 (p44/42 MAPK,
692 #4695), anti-phospho-Erk1/2 (#4370), and anti-IGFBP3 (D1U9C, #25864) were from Cell
693 Signaling Technology (Danvers, MA). Anti-VIM (#MA5-11883) was from Thermo Fisher
694 Scientific (Waltham, MA). Anti- PODXL2 (#AF1524), anti-ECM1 (#MAB39371), anti-TIMP2
695 (#AF971) and anti-ADAM8 (#AF1031) were from R&D Systems (Minneapolis, MN). Anti-
696 SRSF3 (#NBP2-76892) was from Novus Biologicals (Centennial, CO). Rabbit polyclonal anti-
697 HPV16 E7 (#GTX133411) was from GeneTex (Irvine, CA).

698 **RAS GTPase Chemi ELISA**

699 RAS GTPase activity in cell lysate of the WT CaSki or ΔPr-A9 cells was determined by RAS
700 GTPase Chemi ELISA Kit (Active Motif, Carlsbad, CA, # 52097) according to the manufacturer
701 protocol. Briefly, 2×10^7 cells were solubilized in 500 µl of Complete Lysis/Binding buffer at
702 4°C for 15 min. Protein concentration of cell extract was then measured by Micro BCA Protein
703 Assay (PIERCE, #23235) after cell debris was removed by centrifuged at 14,000 × g for 10 min.
704 2 µg of GST-Raf-RBD in 50 µl of Complete Lysis/Binding buffer was coated in each well of a
705 96-well plate by incubating for 1 h at 4°C with 100 rpm agitation. After three times of wash, 50
706 µg of extract in 50 µl Complete Lysis/Binding buffer was then added in each well. HeLa (EGF
707 treated) extract was served as a positive control. The plate was incubated for 1 h at room
708 temperature with 100 rpm agitation. The active RAS protein (GST-Raf-RBD binding) in each
709 well was then detected by incubating with primary RAS antibody and three times of wash, and
710 then, HRP-conjugated secondary antibody and three times of wash. Chemiluminescence in each
711 well was read in luminometer by adding 50 µl room-temperature Chemiluminescent Working
712 Solution.

713 **RNA *in situ* Hybridization (RNA-ISH) and Immunofluorescence (IF) Staining**

714

715 Endogenous lnc-FANCI-2 in cervival cancer tissues and their derived cell lines was examined by
716 RNAScope Multiplex Fluorescent V2 Assay (Advanced Cell Diagnostics, Minneapolis, MN,
717 #323100) as described previously [8]. A custom-designed probe targeting to nt 359-1713 of
718 GenBank Acc. No. MT669800.1 transcript for lnc-FANCI-2a-PA2 was utilized. Dual staining of
719 lnc-FANCI-2 and IGFBP RNA was performed according to RNAscope Multplex Fluorescent v2
720 Manual part 2 (#323100), and the channel one probe for IGFBP3 (#310351) and channel three
721 probe for lnc-FANCI-2 (#509061-C3) were applied.

722 For RNA-ISH combined IF staining of MCAM protein, 3×10^5 of CaSki cells were
723 grown on a glass coverslip in a 6-well plate for 24 h before transfection. Plasmid pHBL05
724 containing a long isoform of lnc-FANCI-2a-PA2 (GenBank Acc. No. MT669800.1) were
725 transfected into cells with LipoD 293 DNA in vitro transfection reagent. Cultured Adherent Cell
726 Sample Preparation for the RNAscope Multplex Fluorescent v2 was performed according to a
727 manufacturer protocol (Advanced Cell Diagnostics, Minneapolis, MN, MK-50-010). Briefly, the
728 cells were washed with PBS and fixed by 10% neutral buffered formalin at room temperature for
729 30 min. The cells were washed with PBS three times and dehydrated by 50% ethanol for 5 min,
730 70% ethanol for 5 min, 100% ethanol for 5 min, and 100% ethanol for 10 min. The cells were
731 then rehydrated by 70% ethanol for 2 min, 50% ethanol for 2 min, and PBS for 10 min. The cells
732 were then applied to hydrogen peroxide at RT for 10 min and washed with distilled water for
733 three times. The cells were then applied to Protease III (1:15 dilution with PBS) at RT for 10
734 min. The cells were ready for RNAscope Multplex Fluorescent v2 Manual part 2 (#323100). IF
735 was performed after RNA-ISH but before counterstaining with DAPI. The cells were washed
736 with PBS, and then were blocked with 2% bovine serum albumin (BSA) in PBS for 1 h at 37°C

737 or overnight at 4°C. The cells were incubated with the MCAM primary antibody (ProteinTech,
738 Rosemont, IL, #17564-1-AP, diluted 1:200 in 2% BSA blocking buffer) for 2 h at 37°C. An
739 Alexa Fluor-conjugated secondary antibody (1: 500, ThermoFisher Scientific) was diluted in a
740 blocking solution and incubated for 1 h at 37˚C. The slides were washed with PBS for three
741 times. DAPI was used for nuclei counterstaining before mounting in a Prolong Gold Antifade
742 mounting medium (Thermo Fisher Scientific, #P36934).

743 Confocal images were collected using a Zeiss LSM710 laser-scanning microscope equipped with
744 a 63 × Plan-Apochromat (N.A. 1.4) objective lens. Three dimensional distributions of lnc-
745 FANCI-2 were generated by Z stacks using ZEN 2.3 software (Zeiss).

746 **Isolation of lnc-FANCI-2 RNA-protein complex by RNA Purification (IRPCRP) and LC-**
747 **MS/MS analysis**

748 To identify the lnc-FANCI-2 RNA-associated proteins, we pulled down lnc-FANCI-2 RNA from
749 WT CaSki cells using IRPCRP, a modified ChIRP protocol from the published method [103],
750 followed by mass spectrometry [60]. Briefly, a total of 30 lnc-FANCI-2 anti-sense oligo probes
751 (oLLY496-oLLY525), each with biotinTEG at 3' end, across entire lnc-FANCI-2 RNA
752 (GenBank Acc. No MT669800.1) were designed using the online probe designer
753 (singlemoleculefish.com). Two probe pools were used in IRPCRP assays: the probe pool 1 was
754 the mixed oligos in even numbers (oLLY496
755 /498/500/502/504/506/508/510/512/514/516/518/520/522/524) and the probe pool 2 mixed with
756 the oligos in odd numbers
757 (oLLY497/499/501/503/505/507/509/511/513/515/517/519/521/523/525) (Table S5). CaSki
758 cells were seeded and harvested at 24 h and the cell lysates from 200 million cells were used for
759 each IRPCRP reaction. Instead of formaldehyde crosslink in the standard protocol [103], UV

760 cross-linking (254 nm, energy at 480 mJ/cm^2) was applied in our study to minimize non-specific
761 binding. After UV cross-linking, the cells were lysed on ice in 1× radioimmunoprecipitation
762 assay (RIPA) buffer (Boston Bioproducts, Ashland, MA, #BP-115) (50 mM Tris base/Tris-HCl
763 [pH 7.4], 150 mM NaCl, 0.5% sodium deoxycholate, 0.1% sodium dodecyl sulfate [SDS], 1%
764 NP-40) supplemented with protease inhibitors (complete mini-EDTA-free protease inhibitor
765 cocktail, Millipore Sigma, Burlington, MA, #469315900) and RNase inhibitor (Thermo Fisher
766 Scientific, #AM2694) for 30 min, followed by a brief sonication. The obtained cell lysates were
767 spin for 10 min of centrifugation at 20,000 × g at 4°C and the collected cell lysate supernatants
768 were pre-absorbed with C-1 magnetic beads (Thermo Fisher Scientific, #65002) for 1 h at room
769 temperature before proceeding to oligo probe hybridization.

770 Two different hybridization protocols were used to pull down lnc-FANCI-2 RNA. One
771 had the pre-absorbed cell lysate incubated with two separate probe pools in hybridization buffer
772 (750 mM NaCl, 0.1% SDS, 50 mM Tris-Cl pH 7.0, 1 mM EDTA, 15% formamide) at room
773 temperature overnight and the pre-washed C-1 magnetic beads was then added and incubated for
774 additional 4 h; the other had two separate oligo probe pools immobilized onto pre-washed C-1
775 magnetic beads first at room temperature for 1 h and then mixed with the pre-absorbed cell
776 lysates in hybridization buffer overnight at room temperature, along with the negative control-
777 beads only IRPCRP reaction without oligo probes serving as a control in the modified protocol.
778 After hybridization, the beads were washed with 1× wash buffer (2× NaCl and sodium citrate,
779 0.1% SDS) for 5 times and resuspend in 1 ml lysis buffer. 100 µl beads from each IRPCRP were
780 set aside for RNA isolation of lnc-FANCI-2 pulldown efficiency and the leftover beads were sent
781 for mass spectrometry analysis. The input and IRPCRP RNA were isolated using a MIRNeasy

782 mini kit (Qiagen, #217004) following the standard protocol after proteinase K (Millipore Sigma,
783 #71049) digestion.

784 For mass spectrometry analysis, the IRPCRP beads were processed for trypsin/LysC
785 digestion before submitted to Thermo Scientific Orbitrap Exploris 240 Mass Spectrometer and a
786 Thermo Dionex UltiMate 3000 RSLCnano System for Proteinomics. Peptides from trypsin
787 digestion were loaded onto a peptide trap cartridge at a flow rate of 5 µl/min. The trapped
788 peptides were eluted onto a reversed-phase Easy-Spray Column PepMap RSLC, C18, 2 µM,
789 100A, 75 µm × 250 mm (Thermo Scientific) using a linear gradient of acetonitrile (3-36%) in
790 0.1% formic acid. The elution duration was 110 min at a flow rate of 0.3 µl/min. Eluted peptides
791 from the Easy-Spray column were ionized and sprayed into the mass spectrometer, using a Nano
792 Easy-Spray Ion Source (Thermo Fisher Scientific) under the following settings: spray voltage,
793 1.6 kV, Capillary temperature, 275 °C. Other settings were empirically determined. Raw data
794 files were searched against human protein sequences database using the Proteome Discoverer 2.4
795 software (Thermo Fisher Scientific, San Jose, CA) based on the SEQUEST algorithm. All the
796 protein peptides identified in the IRPCRP pulldowns were summarized in Table S4.

797 **ACKNOWLEDGEMENTS**

798 We thank Louise T. Chow of the University of Alabama at Birmingham for her critical reading
799 of the manuscript. We thank Craig Meyers of Penn State University Hershey Medical Center for
800 providing HPV16- and HPV18- infected raft cultures, Xing Xie and Yang Li of Zhejiang
801 University Women's Hospital of China for cervical tissue sections, and Johannes G. Schweizer
802 from Arbor Vita corporation for anti-HPV16 E6-specific antibodies. This study was supported
803 by the Intramural Research Program of the NIH, National Cancer Institute, Center for Cancer
804 Research.

805 **DATA AVAILABILITY**

806 NCBI GEO database Acc. No. GSE190904 for CaSki cell RNA-seq.

807 **AUTHORS CONTRIBUTIONS:** H. L., L. Y., and Z.M.Z. designed the study. H. L. and L. Y.
808 performed the experiments. H. L., L. Y., V.M., T. M., M. Y., P. J., M.C., D. R. L., and Z.M.Z.
809 analyzed data and participated in the discussion and interpretation of the results. H. L., L. Y., and
810 Z.M.Z drafted the manuscript. H. L., L. Y., and Z.M.Z. revised the manuscript. All authors read
811 and approved of the final manuscript.

812 **DECLARATION OF INTERESTS:** The authors declare no competing interests.

813

814 **REFERENCES**

815

816 1. Bray F, Laversanne M, Sung H, Ferlay J, Siegel RL, Soerjomataram I, Jemal A: **Global cancer**
817 **statistics 2022: GLOBOCAN estimates of incidence and mortality worldwide for 36 cancers in**
818 **185 countries.** *CA Cancer J Clin* 2024, **74:**229-263.
819 2. Bosch FX, Lorincz A, Munoz N, Meijer CJ, Shah KV: **The causal relation between human**
820 **papillomavirus and cervical cancer.** *J Clin Pathol* 2002, **55:**244-265.
821 3. Munoz N, Bosch FX, de Sanjose S, Herrero R, Castellsague X, Shah KV, Snijders PJ, Meijer CJ,
822 International Agency for Research on Cancer Multicenter Cervical Cancer Study G:
823 **Epidemiologic classification of human papillomavirus types associated with cervical cancer.** *N*
824 *Engl J Med* 2003, **348:**518-527.
825 4. Walboomers JM, Jacobs MV, Manos MM, Bosch FX, Kummer JA, Shah KV, Snijders PJ, Peto J,
826 Meijer CJ, Munoz N: **Human papillomavirus is a necessary cause of invasive cervical cancer**
827 **worldwide.** *J Pathol* 1999, **189:**12-19.
828 5. McCredie MR, Sharples KJ, Paul C, Baranyai J, Medley G, Jones RW, Skegg DC: **Natural history of**
829 **cervical neoplasia and risk of invasive cancer in women with cervical intraepithelial neoplasia**
830 **3: a retrospective cohort study.** *Lancet Oncol* 2008, **9:**425-434.
831 6. Niraj J, Farkkila A, D'Andrea AD: **The Fanconi Anemia Pathway in Cancer.** *Annu Rev Cancer Biol*
832 2019, **3:**457-478.
833 7. Hoskins EE, Morris TA, Higginbotham JM, Spardy N, Cha E, Kelly P, Williams DA, Wikenheiser-
834 Brokamp KA, Duensing S, Wells SI: **Fanconi anemia deficiency stimulates HPV-associated**
835 **hyperplastic growth in organotypic epithelial raft culture.** *Oncogene* 2009, **28:**674-685.
836 8. Liu H, Xu J, Yang Y, Wang X, Wu E, Majerciak V, Zhang T, Steenbergen RDM, Wang HK, Banerjee
837 NS, et al: **Oncogenic HPV promotes the expression of the long noncoding RNA lnc-FANCI-2**
838 **through E7 and YY1.** *Proc Natl Acad Sci U S A* 2021, **118:**e2014195118.

9. Santegoets LA, van Baars R, Terlou A, Heijmans-Antonissen C, Swagemakers SM, van der Spek PJ, Ewing PC, van Beurden M, van der Meijden WI, Helmerhorst TJ, Blok LJ: **Different DNA damage and cell cycle checkpoint control in low- and high-risk human papillomavirus infections of the vulva.** *Int J Cancer* 2012, **130:**2874-2885.
10. Hoskins EE, Morreale RJ, Werner SP, Higginbotham JM, Laimins LA, Lambert PF, Brown DR, Gillison ML, Nuovo GJ, Witte DP, et al: **The fanconi anemia pathway limits human papillomavirus replication.** *J Virol* 2012, **86:**8131-8138.
11. Park JW, Pitot HC, Strati K, Spardy N, Duensing S, Grompe M, Lambert PF: **Deficiencies in the Fanconi anemia DNA damage response pathway increase sensitivity to HPV-associated head and neck cancer.** *Cancer Res* 2010, **70:**9959-9968.
12. Park JW, Shin MK, Lambert PF: **High incidence of female reproductive tract cancers in FA-deficient HPV16-transgenic mice correlates with E7's induction of DNA damage response, an activity mediated by E7's inactivation of pocket proteins.** *Oncogene* 2014, **33:**3383-3391.
13. Hietanen S, Lain S, Krausz E, Blattner C, Lane DP: **Activation of p53 in cervical carcinoma cells by small molecules.** *Proc Natl Acad Sci U S A* 2000, **97:**8501-8506.
14. Tommasino M, Accardi R, Caldeira S, Dong W, Malanchi I, Smet A, Zehbe I: **The role of TP53 in Cervical carcinogenesis.** *Hum Mutat* 2003, **21:**307-312.
15. Prior IA, Lewis PD, Mattos C: **A comprehensive survey of Ras mutations in cancer.** *Cancer Res* 2012, **72:**2457-2467.
16. Fernández-Medarde A, Santos E: **Ras in cancer and developmental diseases.** *Genes Cancer* 2011, **2:**344-358.
17. Roman A, Munger K: **The papillomavirus E7 proteins.** *Virology* 2013, **445:**138-168.
18. Vande Pol SB, Klingelhutz AJ: **Papillomavirus E6 oncoproteins.** *Virology* 2013, **445:**115-137.
19. Liu X, Dakic A, Zhang Y, Dai Y, Chen R, Schlegel R: **HPV E6 protein interacts physically and functionally with the cellular telomerase complex.** *Proc Natl Acad Sci U S A* 2009, **106:**18780-18785.
20. Klingelhutz AJ, Foster SA, McDougall JK: **Telomerase activation by the E6 gene product of human papillomavirus type 16.** *Nature* 1996, **380:**79-82.
21. Storey A, Pim D, Murray A, Osborn K, Banks L, Crawford L: **Comparison of the in vitro transforming activities of human papillomavirus types.** *EMBO J* 1988, **7:**1815-1820.
22. Barbosa MS, Schlegel R: **The E6 and E7 genes of HPV-18 are sufficient for inducing two-stage in vitro transformation of human keratinocytes.** *Oncogene* 1989, **4:**1529-1532.
23. Hawley-Nelson P, Vousden KH, Hubbert NL, Lowy DR, Schiller JT: **HPV16 E6 and E7 proteins cooperate to immortalize human foreskin keratinocytes.** *EMBO J* 1989, **8:**3905-3910.
24. Munger K, Phelps WC, Bubb V, Howley PM, Schlegel R: **The E6 and E7 genes of the human papillomavirus type 16 together are necessary and sufficient for transformation of primary human keratinocytes.** *J Virol* 1989, **63:**4417-4421.
25. Halbert CL, Demers GW, Galloway DA: **The E7 gene of human papillomavirus type 16 is sufficient for immortalization of human epithelial cells.** *J Virol* 1991, **65:**473-478.
26. Phelps WC, Yee CL, Munger K, Howley PM: **The human papillomavirus type 16 E7 gene encodes transactivation and transformation functions similar to those of adenovirus E1A.** *Cell* 1988, **53:**539-547.
27. DiPaolo JA, Woodworth CD, Popescu NC, Notario V, Doniger J: **Induction of human cervical squamous cell carcinoma by sequential transfection with human papillomavirus 16 DNA and viral Harvey ras.** *Oncogene* 1989, **4:**395-399.
28. Schreiber K, Cannon RE, Karrison T, Beck-Engeser G, Huo D, Tennant RW, Jensen H, Kast WM, Krausz T, Meredith SC, et al: **Strong synergy between mutant ras and HPV16 E6/E7 in the development of primary tumors.** *Oncogene* 2004, **23:**3972-3979.

887 29. Narisawa-Saito M, Yoshimatsu Y, Ohno S, Yugawa T, Egawa N, Fujita M, Hirohashi S, Kiyono T: **An**
888 **in vitro multistep carcinogenesis model for human cervical cancer.** *Cancer Res* 2008, **68:**5699-
889 5705.
890 30. Conover CA, Bale LK, Durham SK, Powell DR: **Insulin-like growth factor (IGF) binding protein-3**
891 **potentiation of IGF action is mediated through the phosphatidylinositol-3-kinase pathway and**
892 **is associated with alteration in protein kinase B/AKT sensitivity.** *Endocrinology* 2000, **141:**3098-
893 3103.
894 31. Allard JB, Duan C: **IGF-Binding Proteins: Why Do They Exist and Why Are There So Many?** *Front*
895 *Endocrinol (Lausanne)* 2018, **9:**117.
896 32. Bach LA: **IGF-binding proteins.** *J Mol Endocrinol* 2018, **61:**T11-t28.
897 33. Song S, Pitot HC, Lambert PF: **The human papillomavirus type 16 E6 gene alone is sufficient to**
898 **induce carcinomas in transgenic animals.** *J Virol* 1999, **73:**5887-5893.
899 34. Herber R, Liem A, Pitot H, Lambert PF: **Squamous epithelial hyperplasia and carcinoma in mice**
900 **transgenic for the human papillomavirus type 16 E7 oncogene.** *J Virol* 1996, **70:**1873-1881.
901 35. Song S, Liem A, Miller JA, Lambert PF: **Human papillomavirus types 16 E6 and E7 contribute**
902 **differently to carcinogenesis.** *Virology* 2000, **267:**141-150.
903 36. Riley RR, Duensing S, Brake T, Munger K, Lambert PF, Arbeit JM: **Dissection of human**
904 **papillomavirus E6 and E7 function in transgenic mouse models of cervical carcinogenesis.**
905 *Cancer Res* 2003, **63:**4862-4871.
906 37. Brake T, Lambert PF: **Estrogen contributes to the onset, persistence, and malignant**
907 **progression of cervical cancer in a human papillomavirus-transgenic mouse model.** *Proc Natl*
908 *Acad Sci U S A* 2005, **102:**2490-2495.
909 38. Kato S, Endoh H, Masuhiro Y, Kitamoto T, Uchiyama S, Sasaki H, Masushige S, Gotoh Y, Nishida E,
910 Kawashima H, et al: **Activation of the estrogen receptor through phosphorylation by mitogen-**
911 **activated protein kinase.** *Science* 1995, **270:**1491-1494.
912 39. Statello L, Guo CJ, Chen LL, Huarte M: **Gene regulation by long non-coding RNAs and its**
913 **biological functions.** *Nat Rev Mol Cell Biol* 2021, **22:**96-118.
914 40. Liu H, Zheng ZM: **Linking a nuclear lncRNA to cytoplasmic lysosome integrity and cell death.**
915 *Proc Natl Acad Sci U S A* 2022, **119:**e2123082119.
916 41. Scheffner M, Münger K, Byrne JC, Howley PM: **The state of the p53 and retinoblastoma genes**
917 **in human cervical carcinoma cell lines.** *Proceedings of the National Academy of Sciences* 1991,
918 **88:**5523-5527.
919 42. BeltCappellino A, Majerciak V, Lobanov A, Lack J, Cam M, Zheng ZM: **CRISPR/Cas9-Mediated**
920 **Knockout and In Situ Inversion of the ORF57 Gene from All Copies of the Kaposi's Sarcoma-**
921 **Associated Herpesvirus Genome in BCBL-1 Cells.** *J Virol* 2019, **93:**e00628-00619.
922 43. Schlomann U, Wildeboer D, Webster A, Antropova O, Zeuschner D, Knight CG, Docherty AJ,
923 Lambert M, Skelton L, Jockusch H, Bartsch JW: **The metalloprotease disintegrin ADAM8.**
924 **Processing by autocatalysis is required for proteolytic activity and cell adhesion.** *J Biol Chem*
925 2002, **277:**48210-48219.
926 44. Conrad C, Yildiz D, Cleary SJ, Margraf A, Cook L, Schlomann U, Panaretou B, Bowser JL,
927 Karmouty-Quintana H, Li J, et al: **ADAM8 signaling drives neutrophil migration and ARDS**
928 **severity.** *JCI Insight* 2022, **7**:e149870.
929 45. Liberzon A, Birger C, Thorvaldsdottir H, Ghandi M, Mesirov JP, Tamayo P: **The Molecular**
930 **Signatures Database (MSigDB) hallmark gene set collection.** *Cell Syst* 2015, **1:**417-425.
931 46. Downward J: **Targeting RAS signalling pathways in cancer therapy.** *Nat Rev Cancer* 2003, **3:**11-
932 22.
933 47. Simanshu DK, Nissley DV, McCormick F: **RAS Proteins and Their Regulators in Human Disease.**
934 *Cell* 2017, **170:**17-33.

935 48. Castellano E, Downward J: **RAS Interaction with PI3K: More Than Just Another Effector**
936 **Pathway.** *Genes Cancer* 2011, **2:**261-274.
937 49. Asati V, Mahapatra DK, Bharti SK: **PI3K/Akt/mTOR and Ras/Raf/MEK/ERK signaling pathways**
938 **inhibitors as anticancer agents: Structural and pharmacological perspectives.** *Eur J Med Chem*
939 2016, **109:**314-341.
940 50. Cuesta C, Arevalo-Alameda C, Castellano E: **The Importance of Being PI3K in the RAS Signaling**
941 **Network.** *Genes (Basel)* 2021, **12:**1094.
942 51. Vanhaesebroeck B, Perry MWD, Brown JR, Andre F, Okkenhaug K: **PI3K inhibitors are finally**
943 **coming of age.** *Nat Rev Drug Discov* 2021, **20:**741-769.
944 52. Favata MF, Horiuchi KY, Manos EJ, Daulerio AJ, Stradley DA, Feeser WS, Van Dyk DE, Pitts WJ,
945 Earl RA, Hobbs F, et al: **Identification of a novel inhibitor of mitogen-activated protein kinase**
946 **kinase.** *J Biol Chem* 1998, **273:**18623-18632.
947 53. Serrano ML, Sánchez-Gómez M, Bravo MM: **Insulin-like growth factor system gene expression**
948 **in cervical scrapes from women with squamous intraepithelial lesions and cervical cancer.**
949 *Growth Horm IGF Res* 2007, **17:**492-499.
950 54. Wang Z, Xu Q, Zhang N, Du X, Xu G, Yan X: **CD146, from a melanoma cell adhesion molecule to**
951 **a signaling receptor.** *Signal Transduct Target Ther* 2020, **5:**148.
952 55. Kebir A, Harhouri K, Guillet B, Liu JW, Foucault-Bertaud A, Lamy E, Kaspi E, Elganfoud N, Vely F,
953 Sabatier F, et al: **CD146 short isoform increases the proangiogenic potential of endothelial**
954 **progenitor cells in vitro and in vivo.** *Circ Res* 2010, **107:**66-75.
955 56. Stalin J, Harhouri K, Hubert L, Garrigue P, Nollet M, Essaadi A, Muller A, Foucault-Bertaud A,
956 Bachelier R, Sabatier F, et al: **Soluble CD146 boosts therapeutic effect of endothelial**
957 **progenitors through proteolytic processing of short CD146 isoform.** *Cardiovasc Res* 2016,
958 **111:**240-251.
959 57. Joshkon A, Heim X, Dubrou C, Bachelier R, Traboulsi W, Stalin J, Fayyad-Kazan H, Badran B,
960 Foucault-Bertaud A, Leroyer AS, et al: **Role of CD146 (MCAM) in Physiological and Pathological**
961 **Angiogenesis-Contribution of New Antibodies for Therapy.** *Biomedicines* 2020, **8:**633.
962 58. Baxter RC: **Insulin-like growth factor binding protein-3 (IGFBP-3): Novel ligands mediate**
963 **unexpected functions.** *J Cell Commun Signal* 2013, **7:**179-189.
964 59. Varma Shrivastav S, Bhardwaj A, Pathak KA, Shrivastav A: **Insulin-Like Growth Factor Binding**
965 **Protein-3 (IGFBP-3): Unraveling the Role in Mediating IGF-Independent Effects Within the Cell.**
966 *Front Cell Dev Biol* 2020, **8:**286.
967 60. Chu C, Chang HY: **ChIRP-MS: RNA-Directed Proteomic Discovery.** *Methods Mol Biol* 2018,
968 **1861:**37-45.
969 61. Gao X, Gao C, Liu G, Hu J: **MAP4K4: an emerging therapeutic target in cancer.** *Cell Biosci* 2016,
970 **6:**56.
971 62. Gao X, Chen G, Gao C, Zhang DH, Kuan SF, Stabile LP, Liu G, Hu J: **MAP4K4 is a novel MAPK/ERK**
972 **pathway regulator required for lung adenocarcinoma maintenance.** *Mol Oncol* 2017, **11:**628-
973 639.
974 63. Gonzalez-Montero J, Rojas CI, Burotto M: **MAP4K4 and cancer: ready for the main stage?** *Front*
975 *Oncol* 2023, **13:**1162835.
976 64. Patterson V, Ullah F, Bryant L, Griffin JN, Sidhu A, Saliganan S, Blaile M, Saenz MS, Smith R,
977 Ellingwood S, et al: **Abrogation of MAP4K4 protein function causes congenital anomalies in**
978 **humans and zebrafish.** *Sci Adv* 2023, **9:**eade0631.
979 65. Roth Flach RJ, Guo CA, Danai LV, Yawe JC, Gujja S, Edwards YJ, Czech MP: **Endothelial Mitogen-**
980 **Activated Protein Kinase Kinase Kinase Kinase 4 Is Critical for Lymphatic Vascular**
981 **Development and Function.** *Mol Cell Biol* 2016, **36:**1740-1749.

982 66. Castello A, Hentze MW, Preiss T: **Metabolic Enzymes Enjoying New Partnerships as RNA-**
983 **Binding Proteins.** *Trends Endocrinol Metab* 2015, **26:**746-757.
984 67. Hentze MW, Castello A, Schwarzl T, Preiss T: **A brave new world of RNA-binding proteins.** *Nat*
985 *Rev Mol Cell Biol* 2018, **19:**327-341.
986 68. Crook T, Storey A, Almond N, Osborn K, Crawford L: **Human papillomavirus type 16 cooperates**
987 **with activated ras and fos oncogenes in the hormone-dependent transformation of primary**
988 **mouse cells.** *Proc Natl Acad Sci U S A* 1988, **85:**8820-8824.
989 69. Matlashewski G, Schneider J, Banks L, Jones N, Murray A, Crawford L: **Human papillomavirus**
990 **type 16 DNA cooperates with activated ras in transforming primary cells.** *EMBO J* 1987,
991 **6:**1741-1746.
992 70. Greenhalgh DA, Wang XJ, Rothnagel JA, Eckhardt JN, Quintanilla MI, Barber JL, Bundman DS,
993 Longley MA, Schlegel R, Roop DR: **Transgenic mice expressing targeted HPV-18 E6 and E7**
994 **oncogenes in the epidermis develop verrucous lesions and spontaneous, rasHa-activated**
995 **papillomas.** *Cell Growth Differ* 1994, **5:**667-675.
996 71. Riou G, Barrois M, Sheng ZM, Duvillard P, Lhomme C: **Somatic deletions and mutations of c-Ha-**
997 **ras gene in human cervical cancers.** *Oncogene* 1988, **3:**329-333.
998 72. Eiben GL, Velders MP, Schreiber H, Cassetti MC, Pullen JK, Smith LR, Kast WM: **Establishment of**
999 **an HLA-A*0201 human papillomavirus type 16 tumor model to determine the efficacy of**
1000 **vaccination strategies in HLA-A*0201 transgenic mice.** *Cancer Res* 2002, **62:**5792-5799.
1001 73. Golijow CD, Mouron SA, Gomez MA, Dulout FN: **Differences in K-ras codon 12 mutation**
1002 **frequency between "high-risk" and "low-risk" HPV-infected samples.** *Gynecol Oncol* 1999,
1003 **75:**108-112.
1004 74. Prokopakis P, Sourvinos G, Koumantaki Y, Koumantakis E, Spandidos DA: **K-ras mutations and**
1005 **HPV infection in cervicitis and intraepithelial neoplasias of the cervix.** *Oncol Rep* 2002, **9:**129-
1006 133.
1007 75. Strickland SW, Vande Pol S: **The Human Papillomavirus 16 E7 Oncoprotein Attenuates AKT**
1008 **Signaling To Promote Internal Ribosome Entry Site-Dependent Translation and Expression of**
1009 **c-MYC.** *J Virol* 2016, **90:**5611-5621.
1010 76. Nieto P, Ambrogio C, Esteban-Burgos L, Gómez-López G, Blasco MT, Yao Z, Marais R, Rosen N,
1011 Chiarle R, Pisano DG, et al: **A Braf kinase-inactive mutant induces lung adenocarcinoma.** *Nature*
1012 2017, **548:**239-243.
1013 77. Yang J, Nie J, Ma X, Wei Y, Peng Y, Wei X: **Targeting PI3K in cancer: mechanisms and advances**
1014 **in clinical trials.** *Mol Cancer* 2019, **18:**26.
1015 78. Saliani M, Mirzaiebadizi A, Javadmanesh A, Siavoshi A, Ahmadian MR: **KRAS-related long**
1016 **noncoding RNAs in human cancers.** *Cancer Gene Ther* 2022, **29:**418-427.
1017 79. Martin JL, Weenink SM, Baxter RC: **Insulin-like growth factor-binding protein-3 potentiates**
1018 **epidermal growth factor action in MCF-10A mammary epithelial cells. Involvement of p44/42**
1019 **and p38 mitogen-activated protein kinases.** *J Biol Chem* 2003, **278:**2969-2976.
1020 80. Józefiak A, Larska M, Pomorska-Mól M, Ruszkowski JJ: **The IGF-1 Signaling Pathway in Viral**
1021 **Infections.** *Viruses* 2021, **13:**1488.
1022 81. Jozefiak A, Pacholska-Bogalska J, Myga-Nowak M, Kedzia W, Kwasniewska A, Luczak M, Kedzia H,
1023 Gozdzicka-Jozefiak A: **Serum and tissue levels of insulin-like growth factor-I in women with**
1024 **dysplasia and HPV-positive cervical cancer.** *Mol Med Rep* 2008, **1:**231-237.
1025 82. Serrano ML, Romero A, Cendales R, Sánchez-Gómez M, Bravo MM: **Serum levels of insulin-like**
1026 **growth factor-I and -II and insulin-like growth factor binding protein 3 in women with**
1027 **squamous intraepithelial lesions and cervical cancer.** *Biomedica* 2006, **26:**258-268.

1028 83. Schäfer B, Marg B, Gschwind A, Ullrich A: **Distinct ADAM metalloproteinases regulate G**
1029 **protein-coupled receptor-induced cell proliferation and survival.** *J Biol Chem* 2004, **279:**47929-
1030 47938.
1031 84. Ohtsu H, Dempsey PJ, Eguchi S: **ADAMs as mediators of EGF receptor transactivation by G**
1032 **protein-coupled receptors.** *Am J Physiol Cell Physiol* 2006, **291:**C1-10.
1033 85. Dang M, Dubbin K, D'Aiello A, Hartmann M, Lodish H, Herrlich A: **Epidermal growth factor (EGF)**
1034 **ligand release by substrate-specific a disintegrin and metalloproteases (ADAMs) involves**
1035 **different protein kinase C (PKC) isoenzymes depending on the stimulus.** *J Biol Chem* 2011,
1036 **286:**17704-17713.
1037 86. Kleino I, Järviluoma A, Hepojoki J, Huovila AP, Saksela K: **Preferred SH3 domain partners of**
1038 **ADAM metalloproteases include shared and ADAM-specific SH3 interactions.** *PLoS One* 2015,
1039 **10:**e0121301.
1040 87. Huang YK, Cheng WC, Kuo TT, Yang JC, Wu YC, Wu HH, Lo CC, Hsieh CY, Wong SC, Lu CH, et al:
1041 **Inhibition of ADAM9 promotes the selective degradation of KRAS and sensitizes pancreatic**
1042 **cancers to chemotherapy.** *Nat Cancer* 2024, **5:**400-419.
1043 88. Sun C, Wu MH, Guo M, Day ML, Lee ES, Yuan SY: **ADAM15 regulates endothelial permeability**
1044 **and neutrophil migration via Src/ERK1/2 signalling.** *Cardiovasc Res* 2010, **87:**348-355.
1045 89. Anfosso F, Bardin N, Frances V, Vivier E, Camoin-Jau L, Sampol J, Dignat-George F: **Activation of**
1046 **human endothelial cells via S-endo-1 antigen (CD146) stimulates the tyrosine phosphorylation**
1047 **of focal adhesion kinase p125(FAK).** *J Biol Chem* 1998, **273:**26852-26856.
1048 90. Dye DE, Karlen S, Rohrbach B, Staub O, Braathen LR, Eidne KA, Coombe DR: **hShroom1 links a**
1049 **membrane bound protein to the actin cytoskeleton.** *Cell Mol Life Sci* 2009, **66:**681-696.
1050 91. Bardin N, Frances V, Combes V, Sampol J, Dignat-George F: **CD146: biosynthesis and production**
1051 **of a soluble form in human cultured endothelial cells.** *FEBS Lett* 1998, **421:**12-14.
1052 92. Xu J, Liu H, Yang Y, Wang X, Liu P, Li Y, Meyers C, Banerjee NS, Wang HK, Cam M, et al: **Genome-**
1053 **Wide Profiling of Cervical RNA-Binding Proteins Identifies Human Papillomavirus Regulation of**
1054 **RNASEH2A Expression by Viral E7 and E2F1.** *mBio* 2019, **10**:e02687-18.
1055 93. Justus CR, Leffler N, Ruiz-Echevarria M, Yang LV: **In vitro cell migration and invasion assays.** *J Vis*
1056 *Exp* 2014, **88:**51046.
1057 94. Yu L, Zheng ZM: **Human Papillomavirus Type 16 Circular RNA Is Barely Detectable for the**
1058 **Claimed Biological Activity.** *mBio* 2022, **13:**e0359421.
1059 95. Dobin A, Davis CA, Schlesinger F, Drenkow J, Zaleski C, Jha S, Batut P, Chaisson M, Gingeras TR:
1060 **STAR: ultrafast universal RNA-seq aligner.** *Bioinformatics* 2013, **29:**15-21.
1061 96. Li B, Dewey CN: **RSEM: accurate transcript quantification from RNA-Seq data with or without a**
1062 **reference genome.** *BMC Bioinformatics* 2011, **12:**323.
1063 97. Harrow J, Frankish A, Gonzalez JM, Tapanari E, Diekhans M, Kokocinski F, Aken BL, Barrell D,
1064 Zadissa A, Searle S, et al: **GENCODE: the reference human genome annotation for The ENCODE**
1065 **Project.** *Genome Res* 2012, **22:**1760-1774.
1066 98. Law CW, Chen Y, Shi W, Smyth GK: **voom: Precision weights unlock linear model analysis tools**
1067 **for RNA-seq read counts.** *Genome Biol* 2014, **15:**R29.
1068 99. Smyth GK: **Linear models and empirical bayes methods for assessing differential expression in**
1069 **microarray experiments.** *Stat Appl Genet Mol Biol* 2004, **3:**Article3.
1070 100. Liberzon A, Subramanian A, Pinchback R, Thorvaldsdottir H, Tamayo P, Mesirov JP: **Molecular**
1071 **signatures database (MSigDB) 3.0.** *Bioinformatics* 2011, **27:**1739-1740.
1072 101. Subramanian A, Tamayo P, Mootha VK, Mukherjee S, Ebert BL, Gillette MA, Paulovich A,
1073 Pomeroy SL, Golub TR, Lander ES, Mesirov JP: **Gene set enrichment analysis: a knowledge-**
1074 **based approach for interpreting genome-wide expression profiles.** *Proc Natl Acad Sci U S A*
1075 2005, **102:**15545-15550.

1076 102. Korotkevich G, Sukhov V, Budin N, Shpak B, Artyomov MN, Sergushichev A: **Fast gene set**
1077 **enrichment analysis.** *bioRxiv* 2021.
1078 103. Chu C, Quinn J, Chang HY: **Chromatin isolation by RNA purification (ChIRP).** *J Vis Exp* 2012**:**3912.

1079

1080 **Figure legends**

1081

1082 **Fig. 1.** Increased expression of lnc-FANCI-2 in HPV16-infected cervical squamous cell
1083 carcinoma tissues and HPV16- and HPV18-infected raft culture tissues. (A and B) Expression
1084 lnc-FANCI-2 (red) in HPV16^{+} cervical squamous cell carcinoma tissues were examined by
1085 RNAscope RNA-ISH analysis. Nuclei were stained with DAPI (blue). The corresponding
1086 regions (A) in H&E staining are shown for the adjacent region from the tumor nest and
1087 histotype. (C) Human foreskin keratinocyte (HFK)-derived raft cultures without (HFK) or with
1088 HPV16 or HPV18 infections (HFK-HPV16 or HFK-HPV18) were examined at day 10 for lnc-
1089 FANCI-2 RNA by RNAscope RNA-ISH analysis. Scale bars: 25 μm in the original figures and
1090 10 μm in the zoomed insets.

1091 **Fig. 2.** Knockout (KO) of lnc-FANCI-2 in CaSki cells affects cell proliferation, colony formation
1092 and migration. (A) Diagram and KO strategies of lnc-FANCI-2 gene. On the figure top is the
1093 lnc-FANCI-2 gene structure and its alternative transcription start sites (TSS) and polyadenylation
1094 sites (pA). TSS2 or pA2 with a heavier arrow are predominately used for lnc-FANCI-2
1095 expression. The lower figure part shows KO strategies. Red slashes represent gRNA-targeted
1096 sites to create genomic DNA deletions by CRISPR-Cas9 technology. Deletion of two YY1-
1097 binding motifs (ΔYY1) led to a deletion of 86-bp DNA fragment. Deletion of lnc-FANCI-2
1098 promoter (ΔPr) led to delete a ~3.3-kb promoter region. Primers (P1-P4) used for PCR screening
1099 were shown as black arrows. (B) PCR screening of single cell clones with homozygous lnc-
1100 FANCI-2 KO, with indicated primer sets diagramed (A). Single cell clones selected from the
1101 cells transfected with an empty vector served as control (Ctrl) cells. (C) Evaluation of lnc-
1102 FANCI-2 KO efficiency in the selected single cell clones (B) by RT-qPCR. (D) Northern blot
1103 validation of lnc-FANCI-2 KO efficiency from the individual single cell clones or the parental

1104 (WT) CaSki cells on polyA$^+$ RNA (enriched from 100 μg of total cell RNA, lanes 1-4) or 10 μg
1105 of total cell RNA (lanes 5-9). Total cell RNA (2 μg) of HEK293T cells with ectopic expression
1106 of two isoforms (short, S or long, L) of lnc-FANCI-2 cDNA served as a control. Antisense oligo
1107 probe P5 (A) labeled with ^{32}P was used for hybridization. GAPDH RNA served as a loading
1108 control and hybridized with a GAPDH-specific oligo probe. (E-F) RNA in situ hybridization
1109 (RNA-ISH) validation of lnc-FANCI-2 KO efficiency by RNAscope technology. Two single cell
1110 clones were examined with red color for lnc-FANCI-2 and blue color for the nucleus (E). Bar
1111 graphs show the copy number of lnc-FANCI-2 per cell in the WT, ΔYY1-D5 or ΔPr-A9 CaSki
1112 cells (each averaged from 200 cells) (F). (G-I) Cell proliferation, colony formation and migration
1113 of WT, ΔYY1-D5 or ΔPr-A9 cells show requirements of lnc-FANCI-2 expression for cell
1114 proliferation, colony formation, and cell invasion of CaSki cells. Representative pictures are
1115 shown from three separate experiments of cell proliferation by CCK8 assay (G), cell colony
1116 formation under 1% methylcellulose solution (H), and cell migration by transwell assay (I) of
1117 WT, ΔYY1-D5 or ΔPr-A9 cells. Cell colonies were stained with crystal violet as described in the
1118 procedure. Numbers of the invaded cells crossed the transwell membrane were quantified and
1119 shown as bar graphs (I). *, $P< 0.05$; **, $P<0.01$; ***, $P<0.001$ by two tailed Student *t* test.

1120 **Fig. 3.** KO of lnc-FANCI-2 in CaSki cells affects expression of cellular soluble receptors. (A)
1121 Dot blots show differentially expressed soluble receptors in ΔPr-A9 cells when compared to
1122 those in the WT CaSki cells. A Proteome Profiler Human sReceptor Array was used to examine
1123 105 cellular soluble receptors. Label in red, upregulated receptors; label in blue, downregulated
1124 receptors. (B) Quantification of differentially expressed and/or released soluble receptors (A) in
1125 ΔPr-A9 cells when compared to those in the WT CaSki cells. Error bar represents standard
1126 deviation of replicates in each proteome array. The dash line indicates the threshold of fold

1127 change (FC) with a score above or below the threshold (-/+ 0.3 FC) being determined as
1128 differentially expressed and/or released receptors. (C) Validation of several differentially
1129 expressed soluble receptors by immunoblot analysis using specific antibodies. Tubulin served as
1130 an internal loading control. * non-specific band in MCAM immunoblot.

1131 **Fig. 4.** Transcriptomic effect of lnc-FANCI-2 KO in CaSki cells by RNA-seq analysis. (A)
1132 RNA-seq reads-coverage maps by IGV showing the expression levels of lnc-FANCI-2 from two
1133 KO cell clones, ΔPr-A9 and ΔYY1-D5, to the WT CaSki cells. one representative coverage
1134 profile of four in each type of cells is shown by IGV. FPKM, fragments per kilobase of transcript
1135 per million. Red slashes represent the deleted genomic region, with validated fourteen lnc-
1136 FANCI-2 RNA isoforms shown below [8]. (B) Similarity in heatmap comparison among ΔPr-
1137 A9, ΔYY1-D5 and WT cells was generated using Limma-normalized counts from each sample
1138 by Pearson complete linkage method. (C) Volcano plot visualization of differentially expressed
1139 genes (DEGs) in ΔPr-A9 and ΔYY1-D5. The genes with the most significant change in the
1140 increased (red) or decreased (blue) expression are indicated. FC, fold change. (D) Venn diagram
1141 depicting the overlapped DEGs between ΔPr-A9 and ΔYY1-D5 cells over the WT CaSki cells.
1142 (E) Heatmap shows overlapped DEGs with FPKM ≥7 in ΔPr-A9 and ΔYY1-D5 cells when
1143 compared with the WT CaSki cells. (F) Validation of selective 12 upregulated or downregulated
1144 DEGs shown in the heatmap by RT-PCR with gene-specific primers in the presence (+) or
1145 absence (-) of reverse transcriptase (RT). GAPDH served as an internal RNA control. Relative
1146 expression level of each gene was calculated based on the band density after normalizing to
1147 GAPDH RNA band, with the expression level in the WT CaSki cells setting as 1. M, a 100-bp
1148 DNA marker. (G) Validation of the upregulated expression of IGFBP3 in ΔPr-A9 cells over the
1149 WT CaSki cells by immunoblot analysis.

1150 **Fig. 5.** Pathway analyses of DEGs identified by RNA-seq. (A) Top 3 upregulated and top 4
1151 downregulated pathways in ΔPr-A9 and ΔYY1-D5 cells over the WT CaSki cells. Data were
1152 generated by Gene set enrichment analysis (GSEA) performed with Hallmark gene sets. NES
1153 stands for normalized enrichment score. (B-E) Each GSEA Enrichment plot shows the
1154 enrichment score and gene hits enriched in ΔPr-A9 cells using Hallmark gene sets,
1155 KRAS_SIGNALING_UP (B), EPITHELIAL_MESENCHYMAL_TRANSITION (C),
1156 INTERFERON_GAMMA_ RESPONSE (D) or INTERFERON_ALPHA_RESPONSE (E). padj,
1157 adjusted p value; Zero crossed 7342, the middle number of total genes in the GSEA at ranking.
1158 The heatmaps below the enrichment plots (B and C) visualize the genes enriched in respective
1159 pathways of KRAS_SIGNALING_UP (B) and
1160 EPITHELIAL_MESENCHYMAL_TRANSITION (C) in ΔPr-A9 cells when compared to the
1161 WT CaSki cells.

1162 **Fig. 6.** CaSki cells with lnc-FANCI-2 KO exhibit activation of RAS signaling pathway. (A)
1163 CaSki cells with lnc-FANCI-2 KO (top, ΔPr-A9 cells) or knockdown (KD, lower) by lnc-
1164 FANCI-2-specific siRNAs display increased RAS GTPase activity when compared to the WT
1165 CaSki cells (top) or the WT cells treated with a nonspecific control siRNA (siNS). The relative
1166 RAS GTPase activity was measured by a RAS GTPase Chemi ELISA assay. *, $P< 0.05$; ***,
1167 $P<0.001$ by two tailed Student *t* test. (B and C) Selective validation of increased expression of
1168 RAS signaling-related downstream genes in lnc-FANCI-2 KO ΔPr-A9 cells (B) over the WT
1169 CaSki cells or lnc-FANCI-2 KD CaSki cells (C) over the WT cells treated with a nonspecific
1170 control siRNA (siNS). Relative expression of the indicated genes in ΔPr-A9 cells in comparison
1171 to the WT cells (B) or in the WT CaSki cells treated for 48 h and 96 h with a nonspecific control
1172 siRNA (siNS) or a siRNA specifically targeting the lnc-FANCI-2 exon 3 (C) were

1173 immunoblotted using the corresponding antibodies as indicated. Tubulin served as an internal
1174 control for each blot. The level of p-Akt or p-Erk was calculated by normalizing to total Akt or
1175 Erk protein and the other proteins by normalizing to tubulin. The protein level in the WT cells or
1176 WT cells treated with siNS set as 1. The KD efficiency of lnc-FANCI-2 RNA (C, top bar graphs)
1177 was examined by RT-qPCR. (D) Effect of blocking RAS signaling on the expression of MCAM
1178 and VIM using PI3K inhibitor LY294002 (20 μM) and MEK inhibitor U0126 (10 μM). The
1179 protein at each time point was immunoblotted with a corresponding antibody. The level of
1180 MCAM or VIM was calculated after normalizing to tubulin. The protein level in ΔPr-A9 cells
1181 without the inhibitor was set as 100%. *, nonspecific protein band. (E) The time dependent cell
1182 viability of the WT CaSki and ΔPr-A9 cells in the presence of 20 μM LY294002 or 10 μM
1183 U0126. Data was obtained in each time point after normalizing to the cells treated with DMSO.
1184 The mean ± SD at each data point was calculated from 6 samples combined from two
1185 independent experiments.

1186 **Fig. 7.** lnc-FANCI-2 is suppressive to the expression of IGFBP3 and MCAM. (A and B)
1187 Transient rescue expression of lnc-FANCI-2 in Δpr-A9 cells inhibits the expression of IGFBP3.
1188 ΔPr-A9 cells were transfected with a major isoform lnc-FANCI-2a-PA2 (GenBank ACC. No.
1189 MT669800.1) cDNA plasmid. lnc-FANCI-2 in red and IGFBP3 RNA in green were detected by
1190 RNAscope RNA-ISH at 24h post transfection using each specific antisense RNA probe and
1191 imaged by confocal microscopy (A). Expression levels of lnc-FANCI-2 RNA and IGFBP3 RNA
1192 in four neighboring cells (B) were measured by signal intensity of a line crossing over the stained
1193 cells in A (white line arrow). (C) Validation of differential expression of MCAM RNA in ΔPr-
1194 A9 cells by RT-PCR in the presence (+) or absence (-) of reverse transcriptase (RT). One pair of
1195 primers with one primer at the exons 11 and the other at exon 13 of MCAM RNA (NM_006500)

1196 were used. GAPDH served as a loading control. (D) The major isoform lnc-FANCI-2a-PA2
1197 repressed the expression of MCAM. ΔPr-A9 cells were transfected with lnc-FANCI-2a-PA2
1198 cDNA plasmid. lnc-FANCI-2 RNA in red was detected by RNAscope ISH and MCAM protein
1199 in green was detected by IF with an anti-MCAM antibody. (E) Expression levels of lnc-FANCI-
1200 2 RNA and MCAM protein in three neighboring cells were measured by signal intensity of a line
1201 crossing over the stained cells (D, white line arrow). (F) Calculation of the expression levels of
1202 MCAM in lnc-FANCI-2 positive cells (n=35) and lnc-FANCI-2 negative cells (n=54) by
1203 fluorescent intensity. (G) Subcellular MCAM distributions in the nucleus (N) and cytoplasm (C)
1204 of WT CaSki cells and ΔPr-A9 by immunoblot analysis. Fractionation efficiency and sample
1205 loading were controlled by cytoplasmic (represented by tubulin) and nuclear (represented by
1206 hnRNP C1/C2) proteins. (H-I) Correlation and survival analysis of lnc-FANCI-2 and MCAM
1207 expression with cervical squamous cell carcinoma (CESC) cases from the cancer genome atlas
1208 (TCGA) datasets by GEPIA web server (http://gepia.cancer-pku.cn/). The negative correlation at
1209 R= -0.321 (with p-value=1.02e-08) of lnc-FANCI-2 with MCAM in cervical cancer patients was
1210 obtained from the RNA-seq data from the TCGA CESC tumors downloaded from the TCGA
1211 data portal (https://portal.gdc.cancer.gov/). Only primary solid tumor samples (n=304 after
1212 exclusion of 2 metastatic samples and 3 normal samples) were subjected to analysis, with the
1213 data showing as a Scatter plot (H). Kaplan-Meier plot with log rank test p-value at 5.74e-05 (I)
1214 shows MCAM as a biomarker for poor prognosis of cervical cancer survival with a lower
1215 quartile group cutoff. RNA-seq and survival data are derived from the TCGA CESC cancer
1216 patients. (J/K) AKT and ERK phosphorylation is partially regulated by MCAM and IGFBP3 in
1217 CaSki cells. KD of MCAM (J) and IGFBP3 (K) expression in WT parental CaSki or ΔPr-A9
1218 cells was treated with MCAM siRNA or IGFBP3 siRNA along with or without lnc-FANCI-2

1219 siRNA for 48 h. Expression levels of individual proteins were immunoblotted using the
1220 corresponding antibodies. The level of MCAM, p-Akt, or p-Erk1/2 was calculated after
1221 normalizing to tubulin. The protein level in a non-targeting siRNA (siNS) control set as 1.

1222 **Fig. 8.** lnc-FANCI-2 interacts with host factors to regulate RAS signaling pathway. (A) The lnc-
1223 FANCI-2-associated proteins in the WT CaSki cells were identified by isolation of RNA-protein
1224 complexes using RNA purification (IRPCRP)-mass spectrometry technology. (B) lnc-FANCI-2
1225 RNA in the IRPCRP-1 and IRPCRP-2 pulldowns had the pooled antisense biotinylated oligos
1226 (pool 1 with oligos in even numbers and pool 2 with oligos in odd numbers) immobilized to
1227 avidin-beads first before mixed with cell lysates, while the IRPCRP-3 and IRPCRP-4 pulldowns
1228 had the oligos pool 1 and 2 separately mixed with cell lysates first before addition to the avidin-
1229 beads for the RNA pull-downs. RT-PCR in the absence (-) or presence (+) of reverse
1230 transcriptase (RT) was carried out using the RNA isolated from the individual IRPCRP
1231 experiments using a primer pair of oHBL5 and oHBL12 (Table S5) specific for lnc-FANCI-2
1232 RNA detection. Beads only (no oligos) IRPCRP experiments served as a negative control. Total
1233 RNA from the WT CaSki cells after sonication was used as an input control. The arrow indicates
1234 the detected lnc-FANCI-2 RNA. (C) Proteins associated with lnc-FANCI-2 RNA identified from
1235 lnc-FANCI-2 IRPCRP pulldowns. A total of 32 proteins were specifically pulled down from lnc-
1236 FANCI-2 IRPCRP reactions 1-4 (PSM≥2 from two separate pulldowns, Table S4), with top 10
1237 proteins binding lnc-FANCI-2 shown in the order by the number of identified PSM (peptide
1238 spectrum match) in LC-MS/MS. (D) Expression of p-Akt and p-Erk from CaSki WT cells 48 h
1239 after siRNA KD of MAP4K4 or lnc-FANCI-2 was immunoblotted by the corresponding
1240 antibodies. GAPDH served as a sample loading control. Fold change of the indicated proteins in
1241 the cells with KD of MAP4K4 or lnc-FANCI-2 over the cells treated by a non-targeting siRNA

1242 (siNS) was calculated after normalizing to GAPDH. (E) A proposed model illustrates how lnc-
1243 FANCI-2-protein complexes inhibit the RAS signaling pathway to control Akt/Erk
1244 phosphorylation and expression of host genes. RAS signaling can be regulated by integrating
1245 external and internal factors. In HR-HPV infected cells, viral oncoprotein E7-YY1 complex
1246 transactivates lnc-FANCI-2 expression. By interactions with cellular RBPs, the lnc-FANCI-2-
1247 protein complex inhibits RAS signaling. In the absence of lnc-FANCI-2, increased RAS
1248 signaling leads to phosphorylation of Akt and Erk and cascaded responses of transcription
1249 factors (TFs) and thus regulates the expression of RAS signaling responder genes, such as
1250 IGFBP3, MCAM, etc. Consequently, this brings fundamental biochemical and biological
1251 processes under control by finetuning the RAS pathway.

1252

1253 **Supporting Tables**

1254 **Table S1.** Genome-wide Effect of lnc-FANCI-2 KO in ΔPr-A9 and ΔYY1 cells on gene
1255 expression when compared with parental WT CaSki cells.

1256 **Table S2**. The genes with altered expression found in both ΔPr-A9 and ΔYY1-D5 cells when
1257 compared with parental WT CaSki cells.

1258 **Table S3.** The genes with increased expression in KRAS signaling and EMT and with decreased
1259 expression in IFN-gamma and IFN-alpha responses in lnc-FANCI-2 KO cells (ΔPr-A9 and
1260 ΔYY1-D5) over the parental WT CaSki cells.

1261 **Table S4.** CaSki proteins and their PSMs identified by lnc-FANCI-2 IRPCRP-LC-MS/MS

1262 **Table S5**. Sequences of oligonucleotides used in this study.

1263 **Supporting Figures**

1264 **Figure S1**. Selective expression of lnc-FANCI-2 RNA in cervical cancer cell lines.

1265 **Figure S2.** lnc-FANCI-2 KO on characteristic CaSki cell growth behavior and morphology
1266 imaged at 24 h after spreading.

1267 **Figure S3.** lnc-FANCI-2 KO on expression of viral oncoproteins and cell senescence.

1268 **Figure S4.** GSEA Enrichment plots show enrichment scores and gene hits enriched in ΔYY1-D5
1269 cells using Hallmark gene sets.

1270 **Figure S5.** Pathway map of RAS Initiative with highlighted differentially expressed genes
1271 (DEGs) in ΔPr-A9 cells vs parental wild type cells.

1272 **Figure S6**. Knockout or Knockdown of lnc-FANCI-2 affects RAS signaling.

1273 **Figure S7**. Expression of IGFBP3, MCAM, MAP4K4 and lnc-FANCI-2.

1274 **Figure S8.** Expression levels of lnc-FANCI-2 and MCAM are significantly associated with
1275 TCGA CESC (cervical squamous cell carcinoma) cancer patients' survival outcome.

Fig. 1

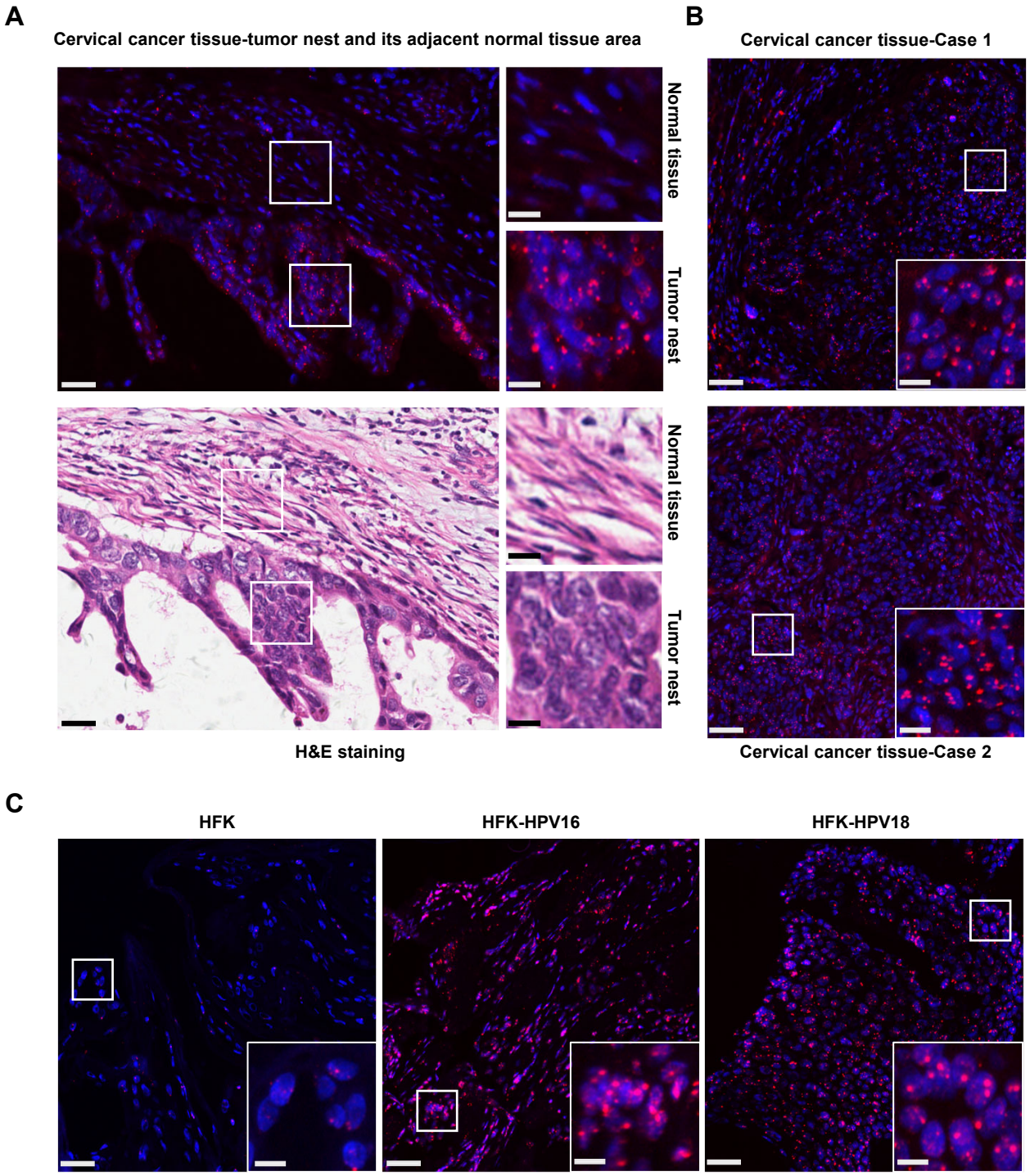
A
Cervical cancer tissue-tumor nest and its adjacent normal tissue area
Normal tissue
Tumor nest
Normal tissue
Tumor nest
H&E staining
B
Cervical cancer tissue-Case 1
Cervical cancer tissue-Case 2
C
HFK
HFK-HPV16
HFK-HPV18

Fig. 2

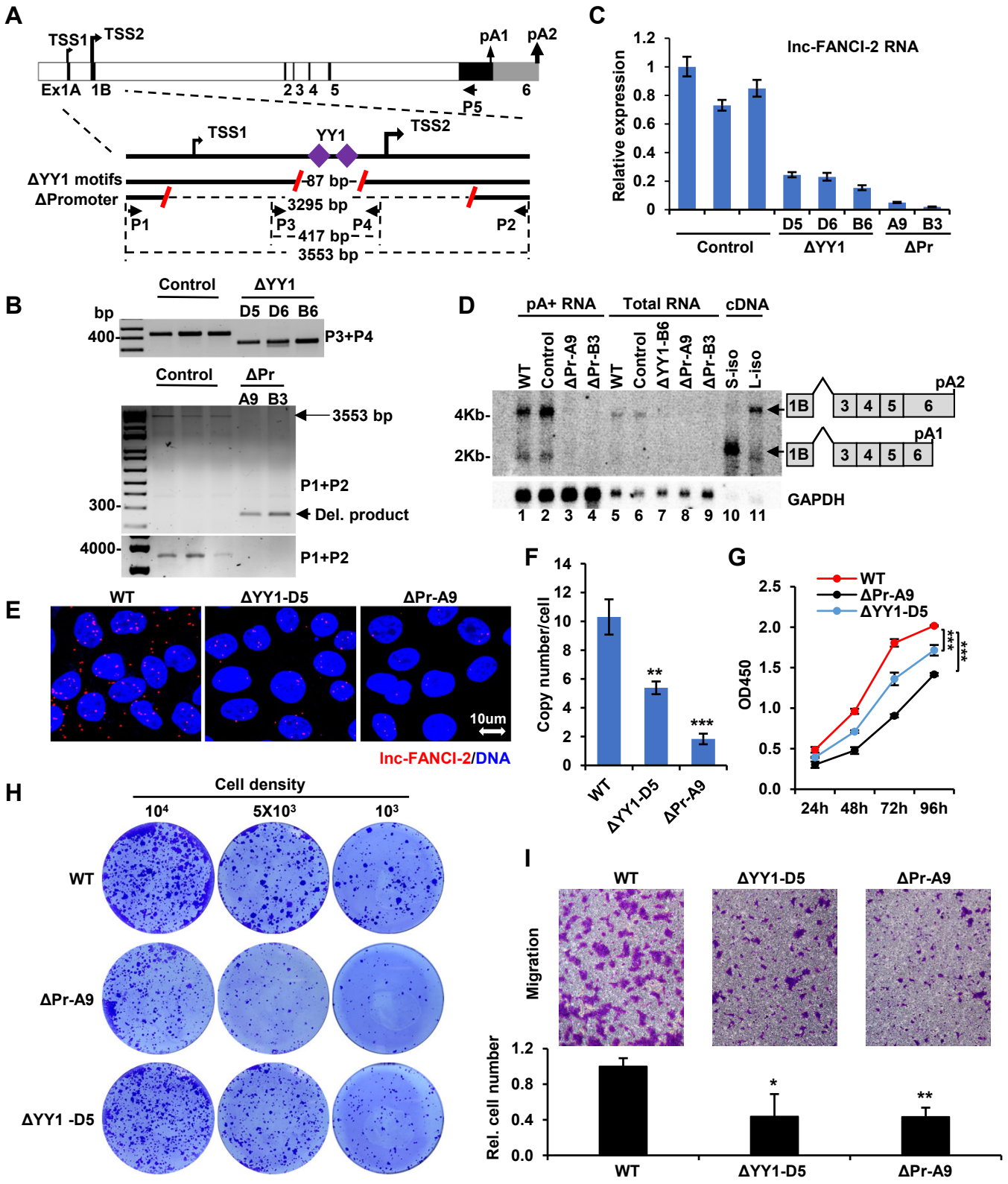
A
TSS1
TSS2
pA1
pA2
Ex1A
1B
2 3 4 5
6
P5
TSS1
YY1
TSS2
ΔYY1 motifs
87 bp
ΔPromoter
3295 bp
P1
P3
P4
P2
417 bp
3553 bp
B
Control
ΔYY1
bp
D5 D6 B6
400-
P3+P4
Control
ΔPr
A9 B3
3553 bp
P1+P2
300-
Del. product
4000-
P1+P2
C
Inc-FANCI-2 RNA
Relative expression
1.2
1
0.8
0.6
0.4
0.2
0
D5 D6 B6 A9 B3
Control
ΔYY1
ΔPr
D
pA+ RNA
Total RNA
cDNA
WT
Control
ΔPr-A9
ΔPr-B3
WT
Control
ΔYY1-B6
ΔPr-A9
ΔPr-B3
S-iso
L-iso
4Kb-
2Kb-
pA2
1B
3 4 5 6
pA1
1B
3 4 5 6
GAPDH
1 2 3 4 5 6 7 8 9 10 11
E
WT
ΔYY1-D5
ΔPr-A9
10um
Inc-FANCI-2/DNA
F
Copy number/cell
14
12
10
8
6
4
2
0
**
***
WT
ΔYY1-D5
ΔPr-A9
G
WT
ΔPr-A9
ΔYY1-D5
OD450
2.5
2.0
1.5
1.0
0.5
0.0
***
***
24h 48h 72h 96h
H
Cell density
10⁴
5X10³
10³
WT
ΔPr-A9
ΔYY1 -D5
I
WT
ΔYY1-D5
ΔPr-A9
Migration
Rel. cell number
1.2
0.8
0.4
0.0
*
**
WT
ΔYY1-D5
ΔPr-A9

Fig. 3

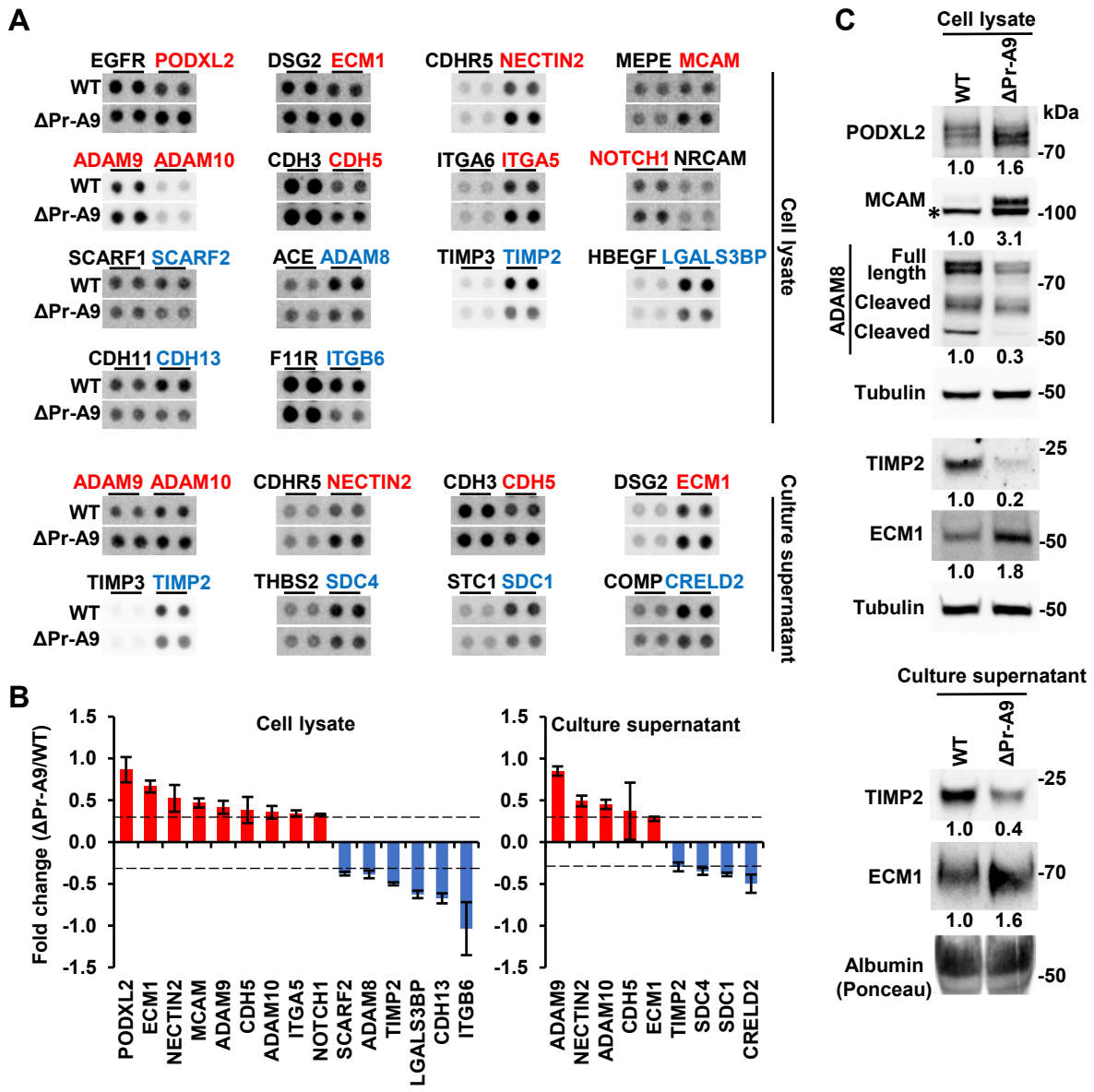
A
EGFR PODXL2
DSG2 ECM1
CDHR5 NECTIN2
MEPE MCAM
ADAM9 ADAM10
CDH3 CDH5
ITGA6 ITGA5
NOTCH1 NRCAM
SCARF1 SCARF2
ACE ADAM8
TIMP3 TIMP2
HBEGF LGALS3BP
CDH11 CDH13
F11R ITGB6
WT
ΔPr-A9
Cell lysate
ADAM9 ADAM10
CDHR5 NECTIN2
CDH3 CDH5
DSG2 ECM1
TIMP3 TIMP2
THBS2 SDC4
STC1 SDC1
COMP CRELD2
Culture supernatant
B
Cell lysate
Culture supernatant
Fold change (ΔPr-A9/WT)
1.5
1.0
0.5
0.0
-0.5
-1.0
-1.5
PODXL2
ECM1
NECTIN2
MCAM
ADAM9
CDH5
ADAM10
ITGA5
NOTCH1
SCARF2
ADAM8
TIMP2
LGALS3BP
CDH13
ITGB6
ADAM9
NECTIN2
ADAM10
CDH5
ECM1
TIMP2
SDC4
SDC1
CRELD2
C
Cell lysate
WT
ΔPr-A9
kDa
PODXL2
-70
1.0 1.6
MCAM
*
-100
1.0 3.1
ADAM8
Full length
Cleaved
Cleaved
-70
-50
1.0 0.3
Tubulin
-50
TIMP2
-25
1.0 0.2
ECM1
-50
1.0 1.8
Tubulin
-50
Culture supernatant
WT
ΔPr-A9
TIMP2
-25
1.0 0.4
ECM1
-70
1.0 1.6
Albumin (Ponceau)
-50

Fig. 4

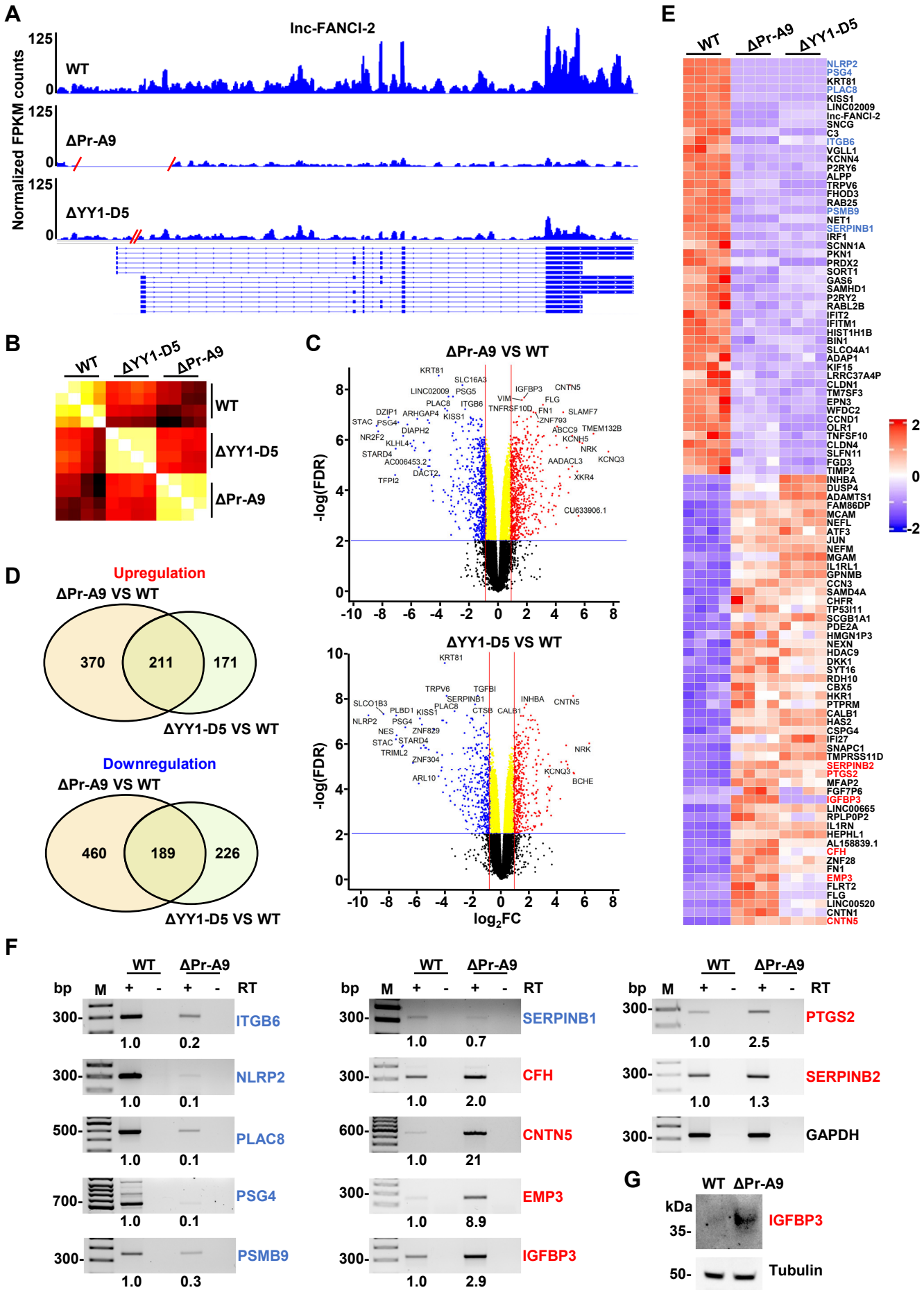
A
lnc-FANCI-2
Normalized FPKM counts
125
0
WT
ΔPr-A9
ΔYY1-D5
B
WT
ΔYY1-D5
ΔPr-A9
C
ΔPr-A9 VS WT
ΔYY1-D5 VS WT
-log(FDR)
log2FC
D
Upregulation
ΔPr-A9 VS WT
370
211
171
ΔYY1-D5 VS WT
Downregulation
460
189
226
E
NLRP2
PSG4
KRT81
PLAC8
KISS1
LINC02009
lnc-FANCI-2
SNCG
C3
ITGB6
VGLL1
KCNN4
P2RY6
ALPP
TRPV6
FHOD3
RAB25
PSMB9
NET1
SERPINB1
IRF1
SCNN1A
PKN1
PRDX2
SORT1
GAS6
SAMHD1
P2RY2
RABL2B
IFIT2
IFITM1
HIST1H1B
BIN1
SLCO4A1
ADAP1
KIF15
LRRC37A4P
CLDN1
TM7SF3
EPN3
WFDC2
CCND1
OLR1
TNFSF10
CLDN4
SLFN11
FGD3
TIMP2
INHBA
DUSP4
ADAMTS1
FAM86DP
MCAM
NEFL
ATF3
JUN
NEFM
MGAM
IL1RL1
GPNMB
CCN3
SAMD4A
CHFR
TP53I11
SCGB1A1
PDE2A
HMGN1P3
NEXN
HDAC9
DKK1
SYT16
RDH10
CBX5
HKR1
PTPRM
CALB1
HAS2
CSPG4
IFI27
SNAPC1
TMPRSS11D
SERPINB2
PTGS2
MFAP2
FGF7P6
IGFBP3
LINC00665
RPLP0P2
IL1RN
HEPHL1
AL158839.1
CFH
ZNF28
FN1
EMP3
FLRT2
FLG
LINC00520
CNTN1
CNTN5
2
0
-2
F
WT
ΔPr-A9
bp
M
+
-
RT
300-
ITGB6
1.0
0.2
NLRP2
1.0
0.1
500-
PLAC8
1.0
0.1
700-
PSG4
1.0
0.1
PSMB9
1.0
0.3
SERPINB1
1.0
0.7
CFH
1.0
2.0
600-
CNTN5
1.0
21
EMP3
1.0
8.9
IGFBP3
1.0
2.9
PTGS2
1.0
2.5
SERPINB2
1.0
1.3
GAPDH
G
kDa
35-
IGFBP3
50-
Tubulin

Fig. 5

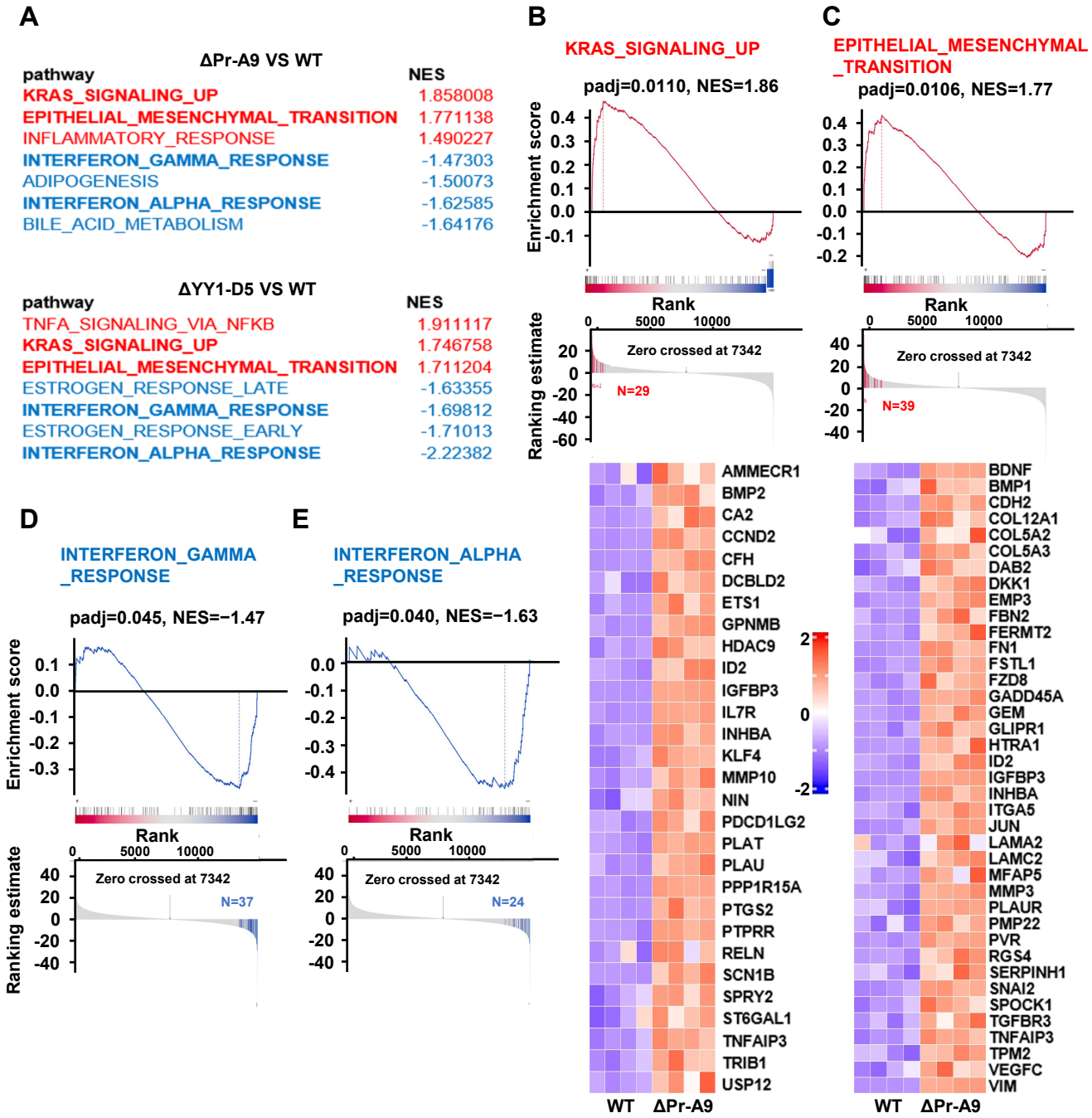
A
ΔPr-A9 VS WT
pathway NES
KRAS_SIGNALING_UP 1.858008
EPITHELIAL_MESENCHYMAL_TRANSITION 1.771138
INFLAMMATORY_RESPONSE 1.490227
INTERFERON_GAMMA_RESPONSE -1.47303
ADIPOGENESIS -1.50073
INTERFERON_ALPHA_RESPONSE -1.62585
BILE_ACID_METABOLISM -1.64176
ΔYY1-D5 VS WT
pathway NES
TNFA_SIGNALING_VIA_NFKB 1.911117
KRAS_SIGNALING_UP 1.746758
EPITHELIAL_MESENCHYMAL_TRANSITION 1.711204
ESTROGEN_RESPONSE_LATE -1.63355
INTERFERON_GAMMA_RESPONSE -1.69812
ESTROGEN_RESPONSE_EARLY -1.71013
INTERFERON_ALPHA_RESPONSE -2.22382
B
KRAS_SIGNALING_UP
padj=0.0110, NES=1.86
Enrichment score
Rank
Ranking estimate
Zero crossed at 7342
N=29
C
EPITHELIAL_MESENCHYMAL_TRANSITION
padj=0.0106, NES=1.77
Zero crossed at 7342
N=39
AMMECR1
BMP2
CA2
CCND2
CFH
DCBLD2
ETS1
GPNMB
HDAC9
ID2
IGFBP3
IL7R
INHBA
KLF4
MMP10
NIN
PDCD1LG2
PLAT
PLAU
PPP1R15A
PTGS2
PTPRR
RELN
SCN1B
SPRY2
ST6GAL1
TNFAIP3
TRIB1
USP12
WT ΔPr-A9
BDNF
BMP1
CDH2
COL12A1
COL5A2
COL5A3
DAB2
DKK1
EMP3
FBN2
FERMT2
FN1
FSTL1
FZD8
GADD45A
GEM
GLIPR1
HTRA1
ID2
IGFBP3
INHBA
ITGA5
JUN
LAMA2
LAMC2
MFAP5
MMP3
PLAUR
PMP22
PVR
RGS4
SERPINH1
SNAI2
SPOCK1
TGFBR3
TNFAIP3
TPM2
VEGFC
VIM
WT ΔPr-A9
D
INTERFERON_GAMMA_RESPONSE
padj=0.045, NES=−1.47
Enrichment score
Rank
Ranking estimate
Zero crossed at 7342
N=37
E
INTERFERON_ALPHA_RESPONSE
padj=0.040, NES=−1.63
Rank
Zero crossed at 7342
N=24

Fig. 6

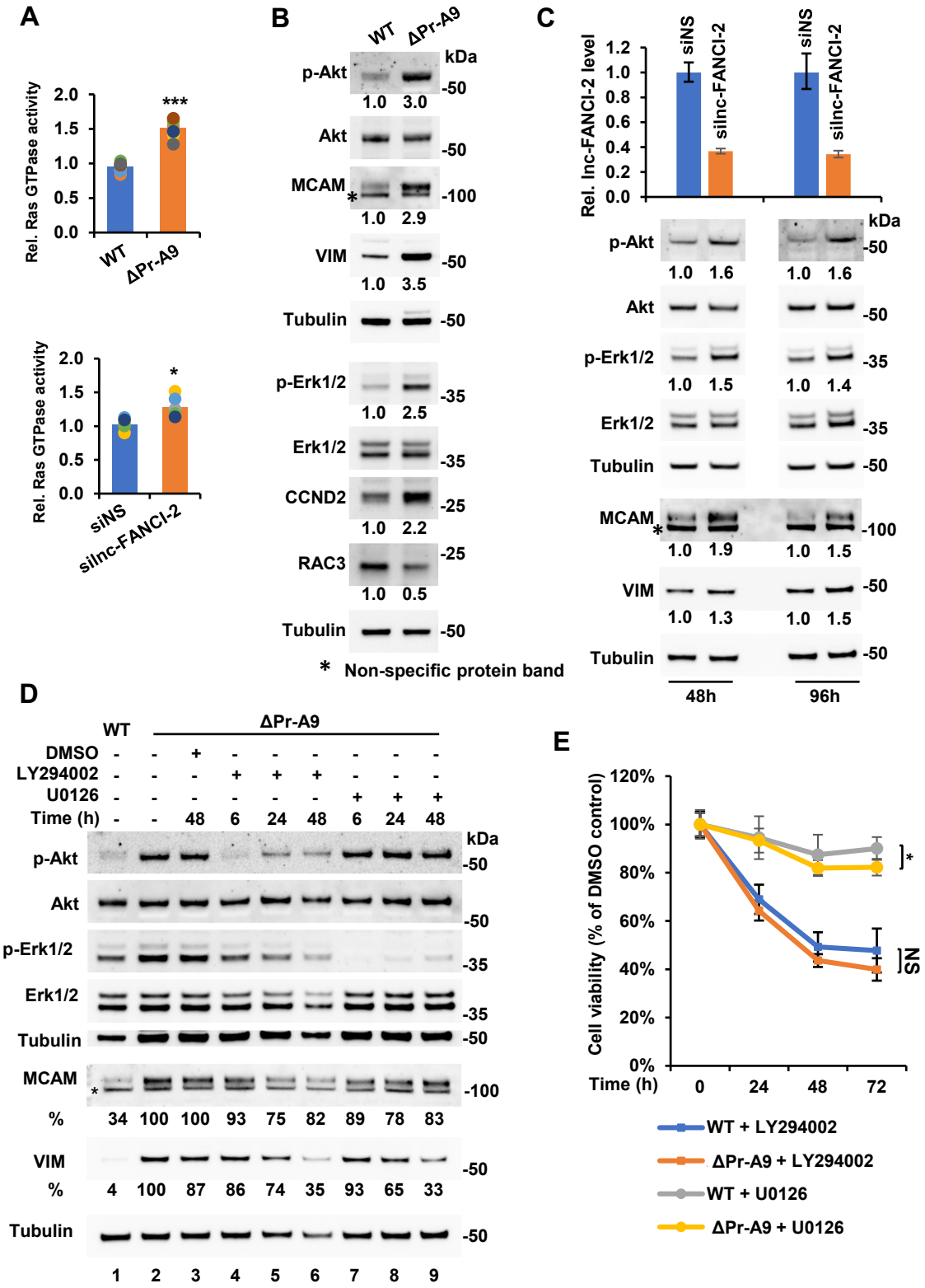
A
Rel. Ras GTPase activity
2.0
1.5
1.0
0.5
0.0
***
WT
ΔPr-A9
Rel. Ras GTPase activity
2.0
1.5
1.0
0.5
0.0
*
siNS
siInc-FANCI-2
B
WT
ΔPr-A9
kDa
p-Akt
1.0 3.0
-50
Akt
-50
MCAM
*
1.0 2.9
-100
VIM
1.0 3.5
-50
Tubulin
-50
p-Erk1/2
1.0 2.5
-35
Erk1/2
-35
CCND2
1.0 2.2
-25
RAC3
1.0 0.5
-25
Tubulin
-50
* Non-specific protein band
C
Rel. lnc-FANCI-2 level
1.2
1.0
0.8
0.6
0.4
0.2
0.0
siNS
siInc-FANCI-2
siNS
siInc-FANCI-2
kDa
p-Akt
1.0 1.6
1.0 1.6
-50
Akt
-50
p-Erk1/2
1.0 1.5
1.0 1.4
-35
Erk1/2
-35
Tubulin
-50
MCAM
*
1.0 1.9
1.0 1.5
-100
VIM
1.0 1.3
1.0 1.5
-50
Tubulin
-50
48h
96h
D
WT
ΔPr-A9
DMSO - - + - - - - - -
LY294002 - - - + + + - - -
U0126 - - - - - - + + +
Time (h) - - 48 6 24 48 6 24 48
kDa
p-Akt
-50
Akt
-50
p-Erk1/2
-35
Erk1/2
-35
Tubulin
-50
MCAM
*
-100
% 34 100 100 93 75 82 89 78 83
VIM
-50
% 4 100 87 86 74 35 93 65 33
Tubulin
-50
1 2 3 4 5 6 7 8 9
E
Cell viability (% of DMSO control)
120%
100%
80%
60%
40%
20%
0%
Time (h)
0
24
48
72
]*
NS
WT + LY294002
ΔPr-A9 + LY294002
WT + U0126
ΔPr-A9 + U0126

Fig. 7

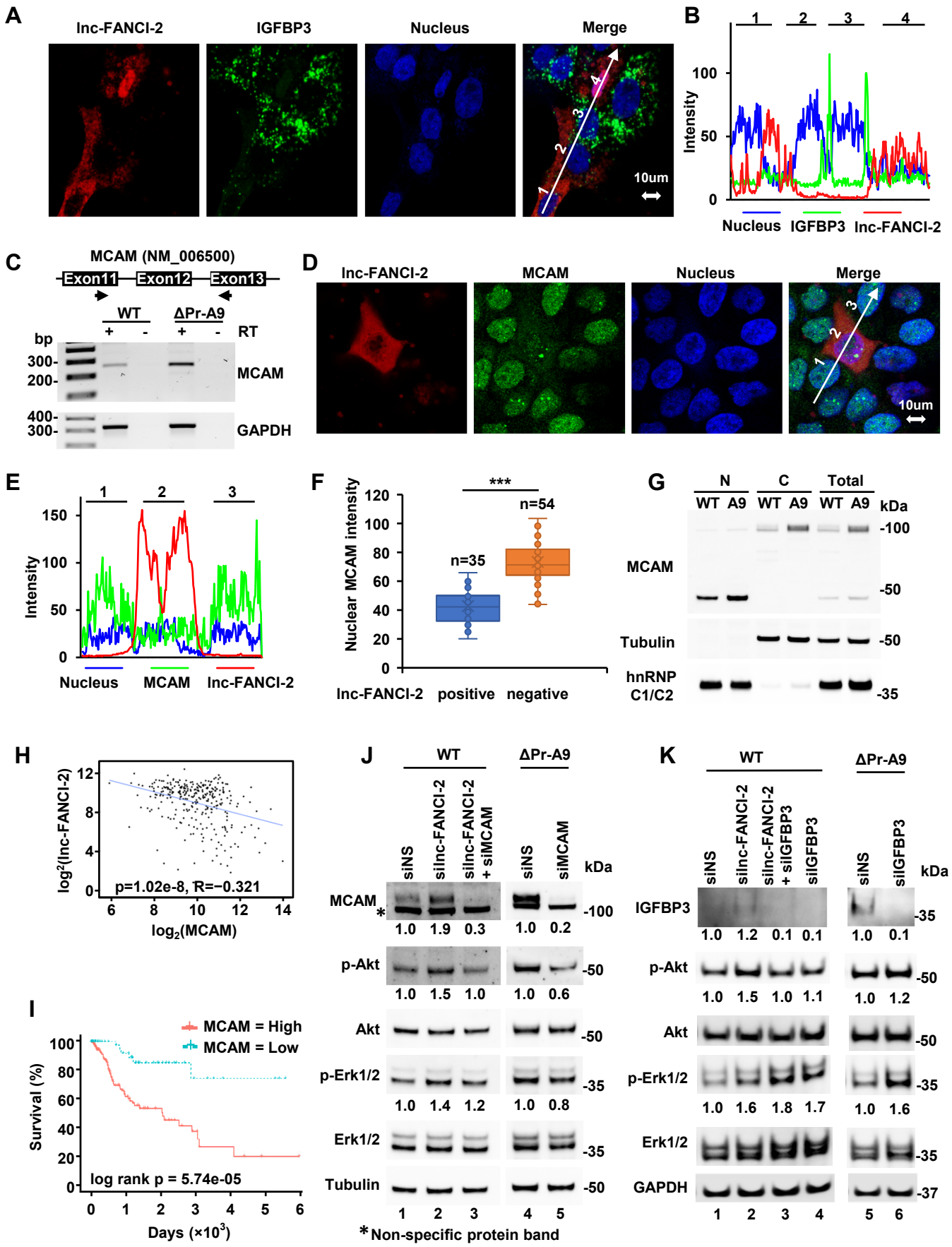
A
lnc-FANCI-2
IGFBP3
Nucleus
Merge
10um
B
Intensity
Nucleus
IGFBP3
lnc-FANCI-2
C
MCAM (NM_006500)
Exon11
Exon12
Exon13
WT
ΔPr-A9
RT
bp
MCAM
GAPDH
D
lnc-FANCI-2
MCAM
Nucleus
Merge
10um
E
Intensity
Nucleus
MCAM
lnc-FANCI-2
F
Nuclear MCAM intensity
n=35
n=54
lnc-FANCI-2
positive
negative
G
N
C
Total
WT
A9
kDa
MCAM
Tubulin
hnRNP C1/C2
H
log2(lnc-FANCI-2)
log2(MCAM)
p=1.02e-8, R=−0.321
I
MCAM = High
MCAM = Low
Survival (%)
log rank p = 5.74e-05
Days (×10³)
J
WT
ΔPr-A9
siNS
siInc-FANCI-2
siInc-FANCI-2 + siMCAM
siMCAM
MCAM
p-Akt
Akt
p-Erk1/2
Erk1/2
Tubulin
*Non-specific protein band
K
siIGFBP3
IGFBP3
GAPDH

Fig. 8

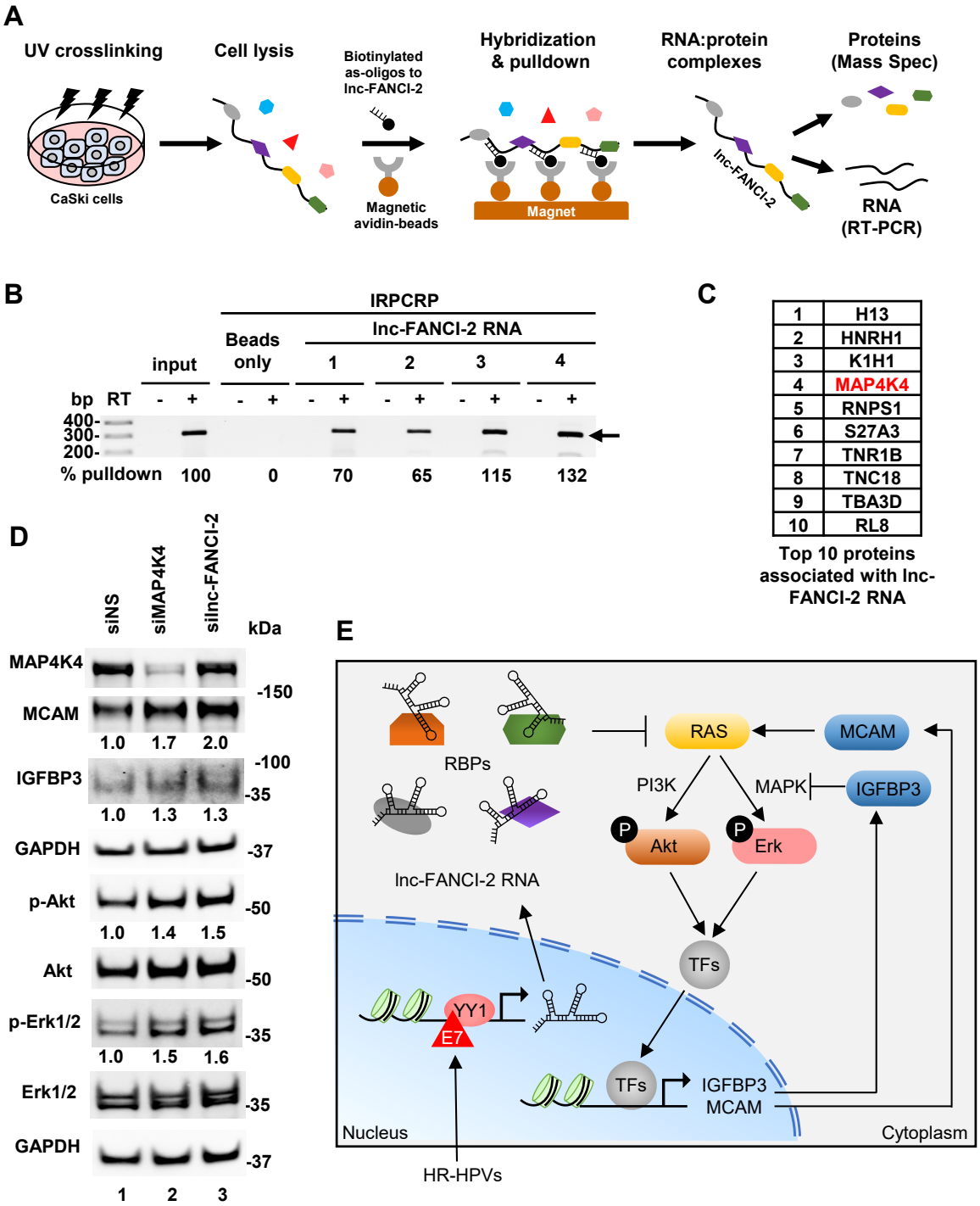
A
UV crosslinking
CaSki cells
Cell lysis
Biotinylated as-oligos to lnc-FANCI-2
Magnetic avidin-beads
Hybridization & pulldown
Magnet
RNA:protein complexes
lnc-FANCI-2
Proteins (Mass Spec)
RNA (RT-PCR)
B
IRPCRP
lnc-FANCI-2 RNA
input
Beads only
1
2
3
4
bp RT - + - + - + - + - + - +
400-
300-
200-
% pulldown 100 0 70 65 115 132
C
1 H13
2 HNRH1
3 K1H1
4 MAP4K4
5 RNPS1
6 S27A3
7 TNR1B
8 TNC18
9 TBA3D
10 RL8
Top 10 proteins associated with lnc-FANCI-2 RNA
D
siNS
siMAP4K4
siInc-FANCI-2
kDa
MAP4K4
-150
MCAM
1.0 1.7 2.0
IGFBP3
-100
-35
1.0 1.3 1.3
GAPDH
-37
p-Akt
-50
1.0 1.4 1.5
Akt
-50
p-Erk1/2
-35
1.0 1.5 1.6
Erk1/2
-35
GAPDH
-37
1 2 3
E
RBPs
RAS
MCAM
PI3K
MAPK
IGFBP3
P
Akt
P
Erk
lnc-FANCI-2 RNA
TFs
YY1
E7
TFs
IGFBP3
MCAM
Nucleus
Cytoplasm
HR-HPVs

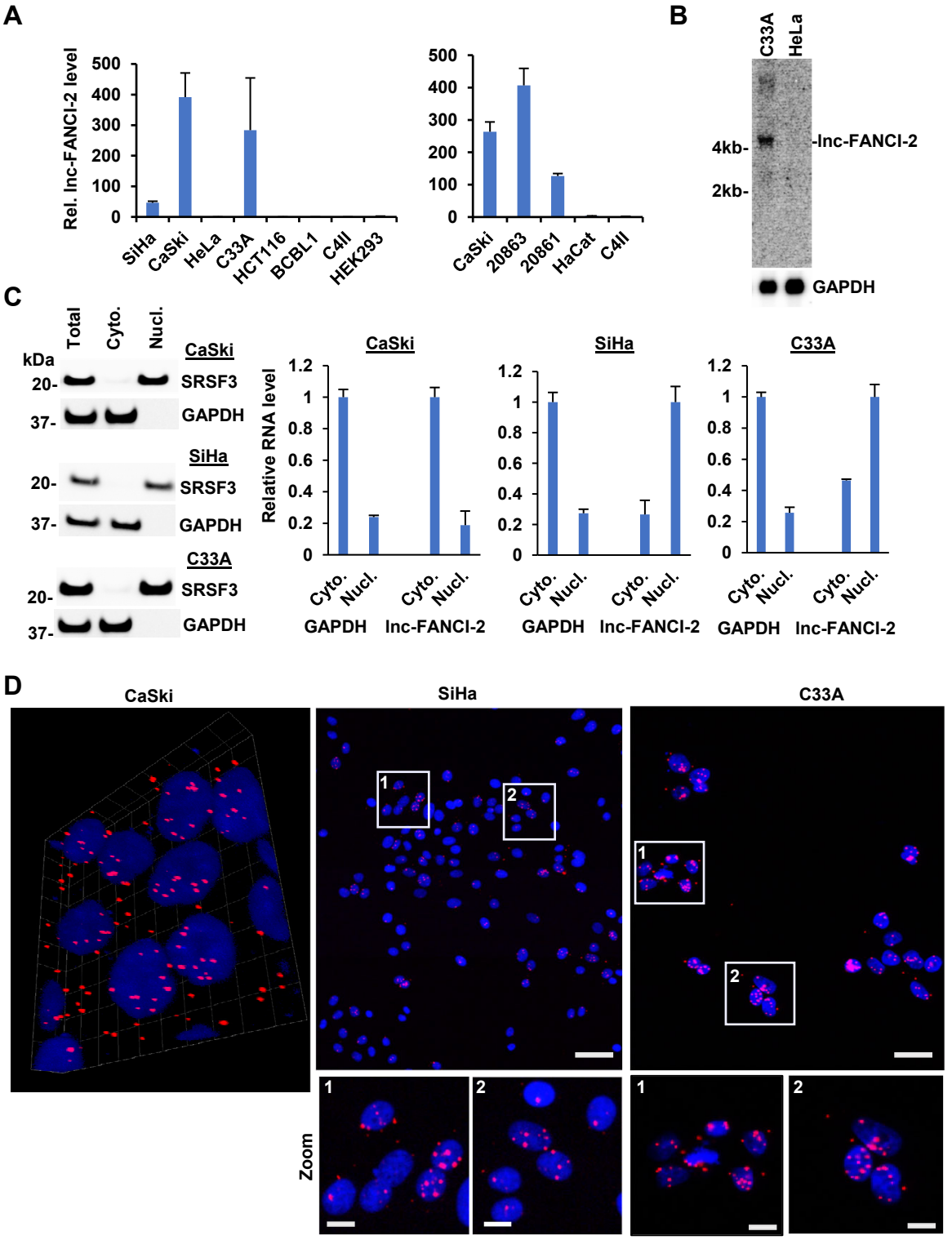

Fig S1. Selective expression of lnc-FANCI-2 RNA in cervical cancer cell lines. (A)) RT-qPCR detection of lnc-FANCI-2 in HPV16^{+} cervical cancer cell lines SiHa, CaSki, and W12 20861 (integrated HPV16) and 20863 (episomal HPV16), HPV18^{+} cervical cancer cell lines HeLa and C4II, and HPV^{-} cell lines C33A (cervical cancer cells with mutations of p53 and pRb), HCT116 (colorectal cancer cells), BCBL-1 (body cavity B lymphoma cells), HEK293 (Ad5 E1/E2-immortalized human kidney cells), and HaCaT (spontaneously immortalized human epidermal cells) in triplicates. (B) HeLa cells express no lnc-FANCI-2 when compared with C33A cells by Northern blot. (C) lnc-FANCI-2 is mainly cytoplasmic in CaSki but nuclear in SiHa and C33A cells. Cytoplasmic and nuclear fractionation efficiency was blotted for nuclear SRSF3 (serine- and arginine-rich splicing factor 3) and cytoplasmic GAPDH. Total fractionated cytoplasmic and nuclear RNAs were quantified for lnc-FANCI-2 by RT-qPCR in triplicates, with GAPDH RNA serving as an internal control for RNA fractionation efficiency. (D) Subcellular lnc-FANCI-2 (red) localization in CaSki, SiHa, and C33A cells determined by RNAscope RNA ISH analysis. Nuclei were stained with DAPI (blue). Scale bars: 25 μm in the top and 10 μm in the zoom.

A

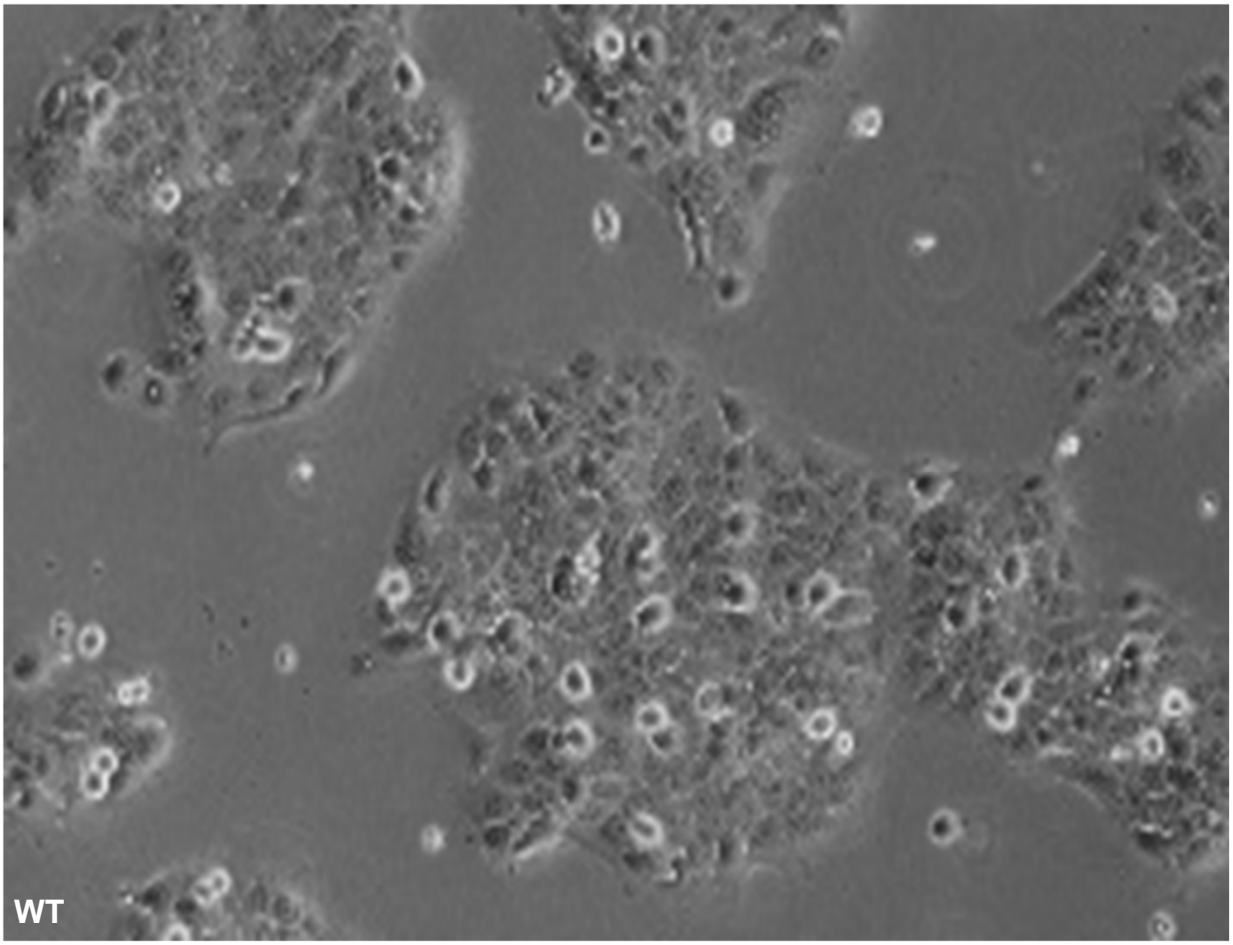

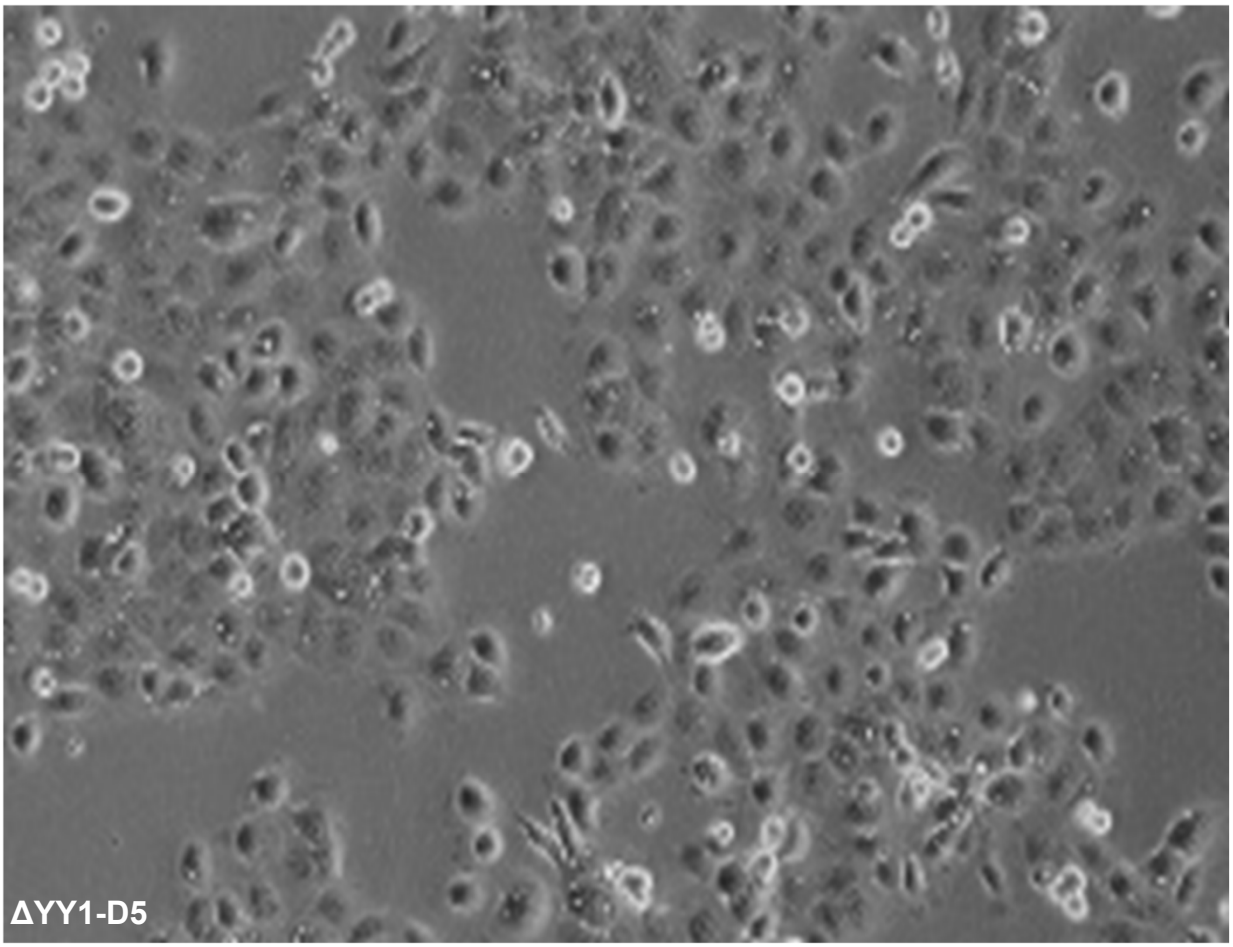

B

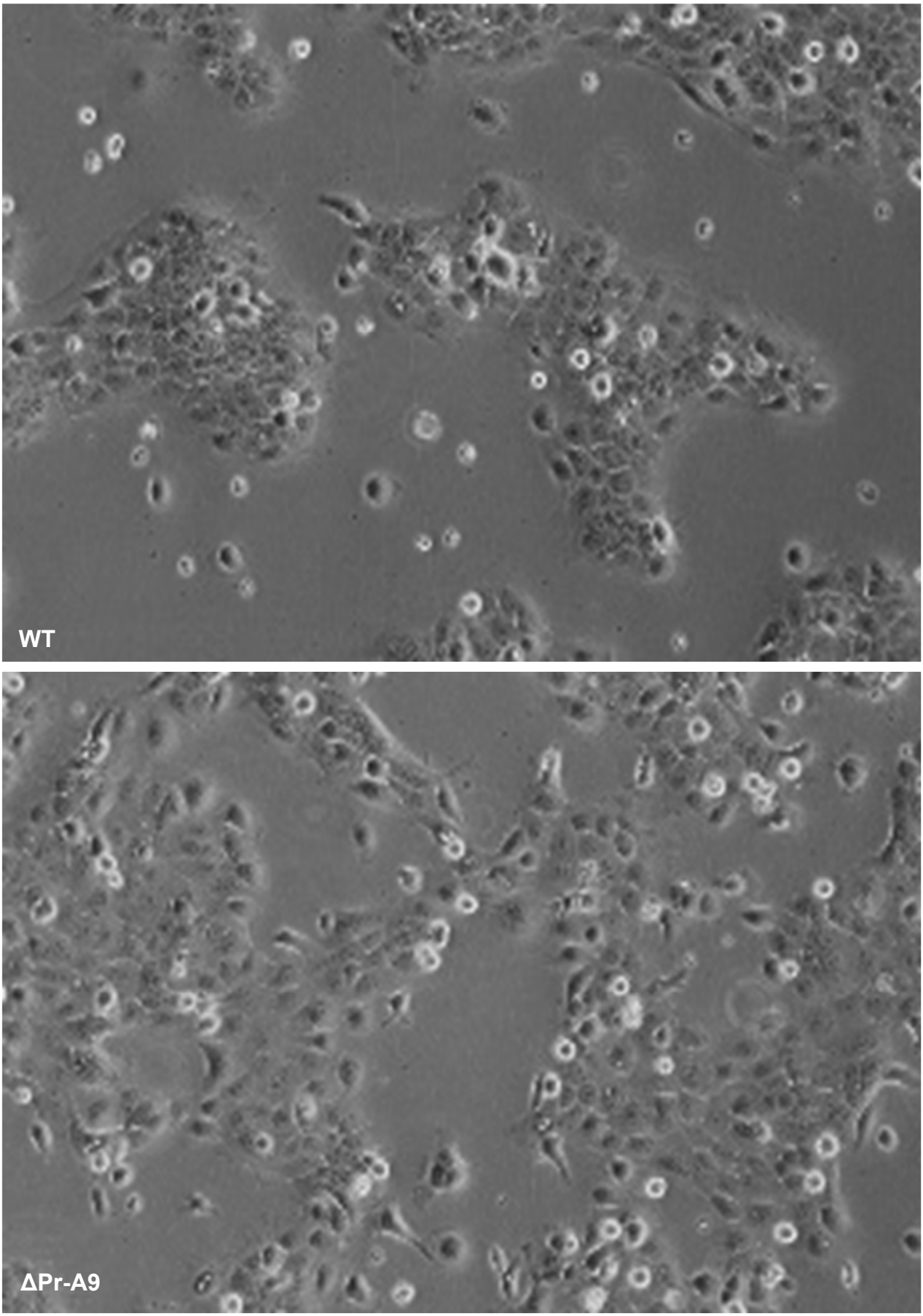

Fig. S2. lnc-FANCI-2 KO on characteristic CaSki cell growth behavior and morphology imaged at 24 h after spreading. (A) Parental WT CaSki and ΔYY1-D5 CaSki cells. (B) Parental WT CaSki and ΔPr-A9 CaSki cells.

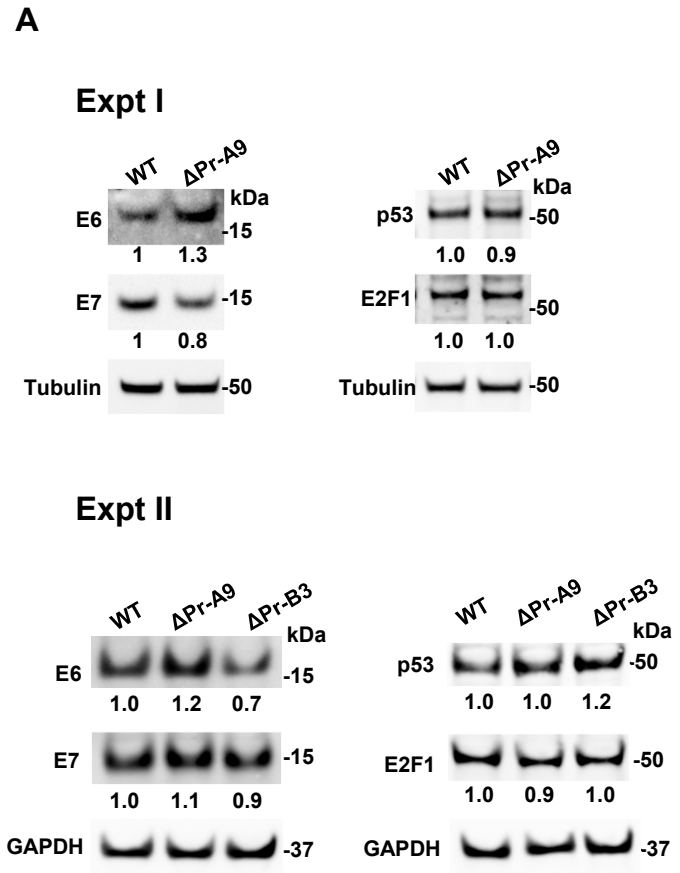

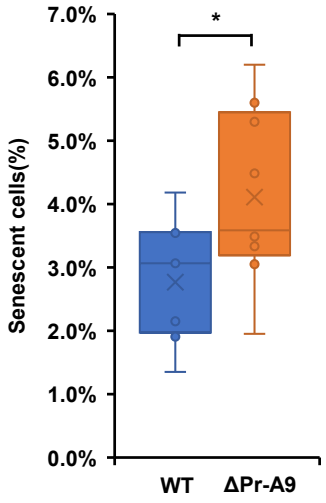

Fig. S3. lnc-FANCI-2 KO on the expression of viral oncoproteins and cell senescence. (A) Effect of lnc-FANCI-2 KO in CaSki cells on the expression of HPV16 E6 and E7 and their downstream targets. Total cell extracts from parental CaSki, ΔPr-A9, and ΔPr-B3 cells were immunobloted with the corresponding antibodies. Tubulin or GAPDH served as a protein loading control. The relative protein levels of E6, E7, p53, and E2F1 were calculated after normalizing to tubulin or GAPDH in the corresponding experiment. Expt I or II = experiment I or II. (B) KO of lnc-FANCI-2 expression enhances cell senescence in β-gal analysis.

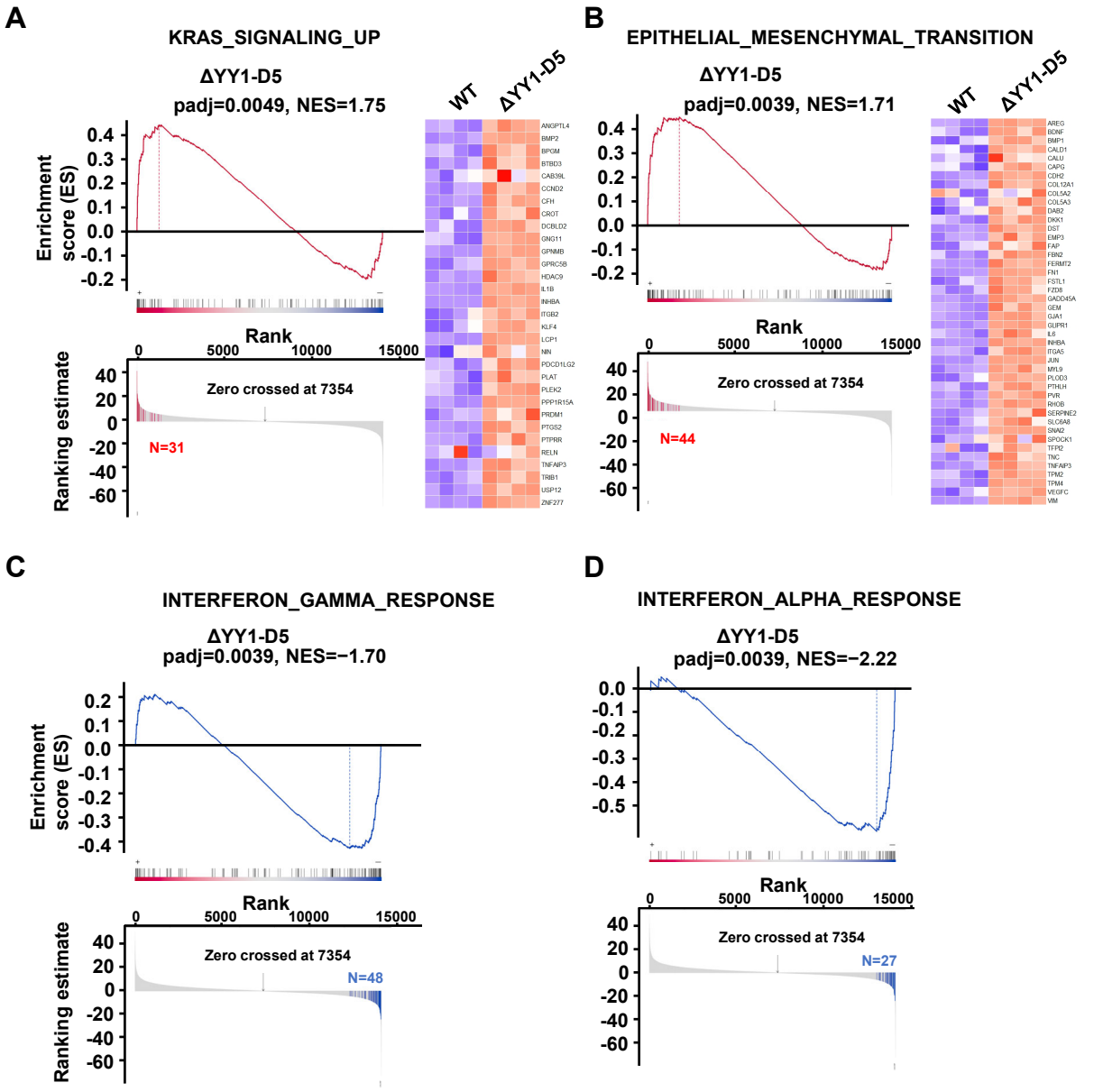

Fig S4. GSEA Enrichment plots show enrichment scores and gene hits enriched in ΔYY1-D5 cells using Hallmark gene sets. (A) KRAS_SIGNALING_UP. (B) EPITHELIAL_MESENCHYMAL_TRANSITION. (C) INTERFERON_GAMMA_RESPONSE. (D) INTERFERON_ALPHA_RESPONSE. The heatmaps on the right side of Enrichment plot in the panels A and B visualize the genes with differentiated expression enriched in each pathway in ΔYY1-D5 cells.

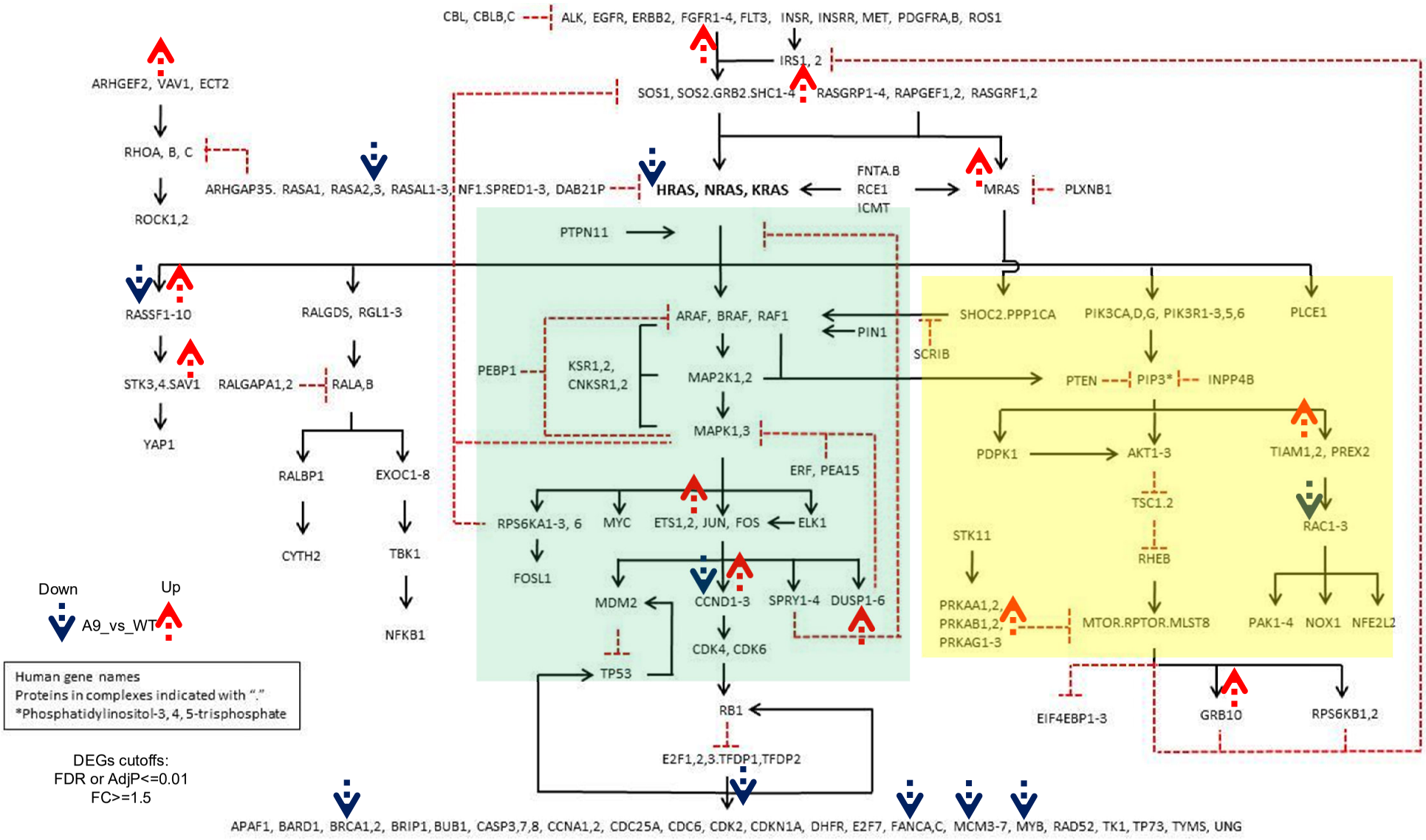
CBL, CBLB,C
ALK, EGFR, ERBB2, FGFR1-4, FLT3, INSR, INSRR, MET, PDGFRA,B, ROS1
IRS1, 2
ARHGEF2, VAV1, ECT2
SOS1, SOS2.GRB2.SHC1-4
RASGRP1-4, RAPGEF1,2, RASGRF1,2
RHOA, B, C
ARHGAP35. RASA1, RASA2,3, RASAL1-3, NF1.SPRED1-3, DAB21P
HRAS, NRAS, KRAS
FNTA.B
RCE1
ICMT
MRAS
PLXNB1
ROCK1,2
PTPN11
RASSF1-10
RALGDS, RGL1-3
ARAF, BRAF, RAF1
PIN1
SHOC2.PPP1CA
PIK3CA,D,G, PIK3R1-3,5,6
PLCE1
SCRIB
PEBP1
KSR1,2,
CNKSR1,2
MAP2K1,2
STK3,4.SAV1
RALGAPA1,2
RALA,B
PTEN
PIP3*
INPP4B
YAP1
MAPK1,3
PDPK1
AKT1-3
TIAM1,2, PREX2
ERF, PEA15
RALBP1
EXOC1-8
TSC1.2
RPS6KA1-3, 6
MYC
ETS1,2, JUN, FOS
ELK1
RAC1-3
STK11
CYTH2
TBK1
RHEB
FOSL1
MDM2
CCND1-3
SPRY1-4
DUSP1-6
PRKAA1,2,
PRKAB1,2,
PRKAG1-3
MTOR.RPTOR.MLST8
PAK1-4
NOX1
NFE2L2
NFKB1
CDK4, CDK6
TP53
RB1
EIF4EBP1-3
GRB10
RPS6KB1,2
E2F1,2,3.TFDP1,TFDP2
APAF1, BARD1, BRCA1,2, BRIP1, BUB1, CASP3,7,8, CCNA1,2, CDC25A, CDC6, CDK2, CDKN1A, DHFR, E2F7, FANCA,C, MCM3-7, MYB, RAD52, TK1, TP73, TYMS, UNG
Down
Up
A9_vs_WT
Human gene names
Proteins in complexes indicated with "."
*Phosphatidylinositol-3, 4, 5-trisphosphate
DEGs cutoffs:
FDR or AdjP<=0.01
FC>=1.5

Fig. S5. Pathway map of RAS Initiative with highlighted differentially expressed genes (DEGs) in ΔPr-A9 cells vs parental wild type cells. DEGs are mainly distributed and clustered in two main branches of RAS pathway: MAPK signaling branch and PI3K/AKT branches. DEGs were derived from RNA-seq data at cutoff of adjusted p-value <=0.01 and fold change>1.5 for both up- and down-regulated genes (indicated by red and blue arrows respectively) between ΔPr-A9 vs WT CaSki cells using three common analysis methods (DESeq2, edgeR, and limma-voom) and in-house BRB analysis pipeline from NCI. Highlighted genes in the pathway map are derived as DEGs in at least three of the analysis methods, although in most cases, these DEGs behaved consistently across all 4 methods. MAPK signaling branch is highlighted in transparent green box and PI3K/AKT branch is highlighted in transparent yellow box within the pathway map of RAS signaling pathway, which was collectively collated from community inputs that were organized and stimulated by RAS Initiative, and maintained as a common knowledge basis at URL below: https://www.cancer.gov/research/key-initiatives/ras/ras-central/blog/2015/ras-pathway-v2, which was also described in recent review (Figure 1 in Nissley and McCormick, 2022).

Reference (where the Ras pathway map has been described):

Nissley, D. V. and McCormick, F. (2022). RAS at 40: update from the RAS Initiative. *Cancer Discov.* https://doi.org/10.1158/2159-8290.CD-21-1554

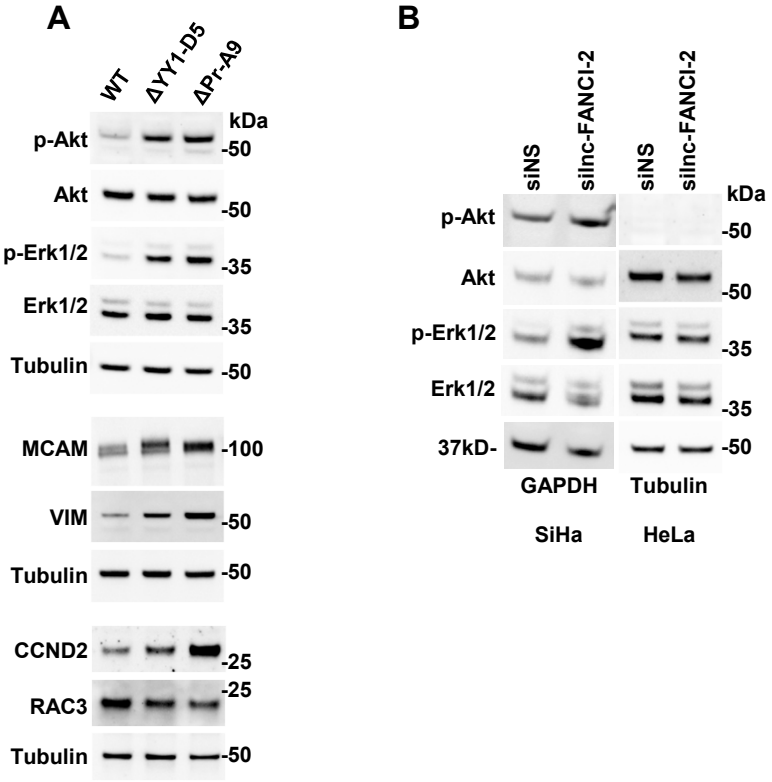

Fig S6. Knockout or Knockdown of lnc-FANCI-2 affects RAS signaling. (A) Selective validation of increased expression of RAS signaling-related downstream genes in ΔPr-A9 and ΔYY1-D5 cells. (B) KD of lnc-FANCI-2 expression in SiHa cells enhanced phosphorylation of Akt and Erk1/2 but did not in HeLa cells expressing no lnc-FANCI-2.

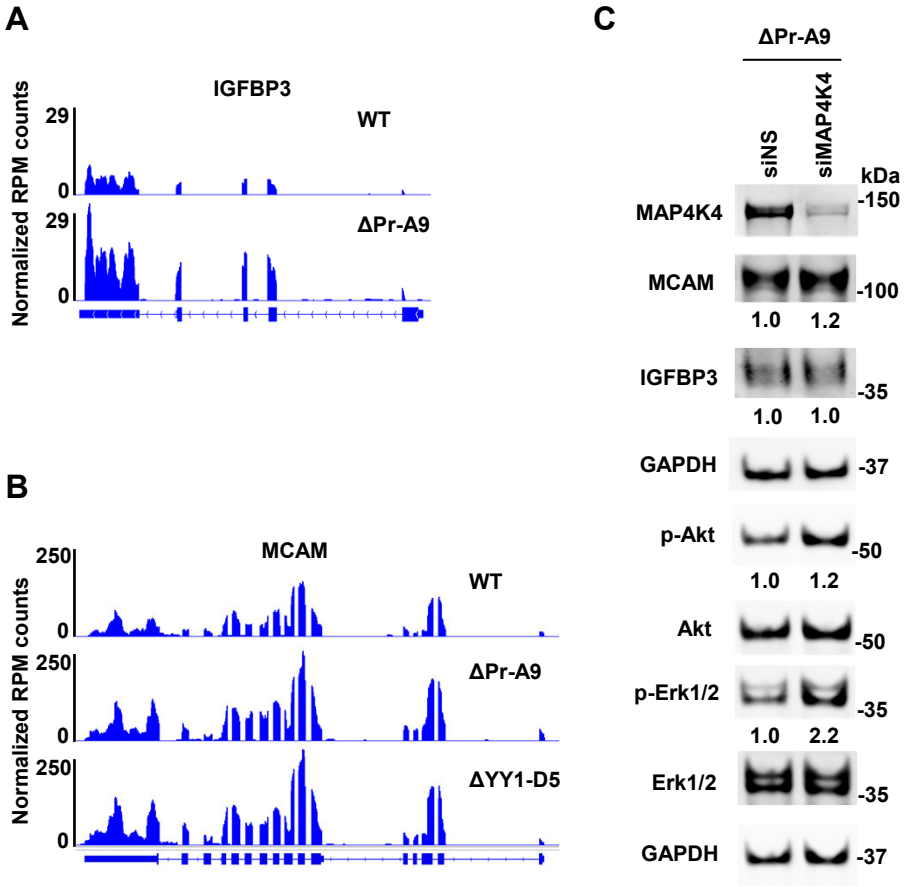

Fig. S7. Expression of IGFBP3, MCAM, and MAP4K4 and lnc-FANCI-2. (A-B) RNA-seq reads-coverage of IGFBP3 and MCAM by IGV illustrates the increased expression of IGFBP3 and MCAM in lnc-FANCI-2 KO cells ΔPr-A9 and/or ΔYY1-D5 when compared to the parental WT CaSki cells. (C) KD of MAP4K4 expression in lnc-FANCI-2 KO ΔPr-A9 cells further enhances phosphorylation of Erk1/2 but little on MCAM and p-Akt and no effect on IGFBP3.

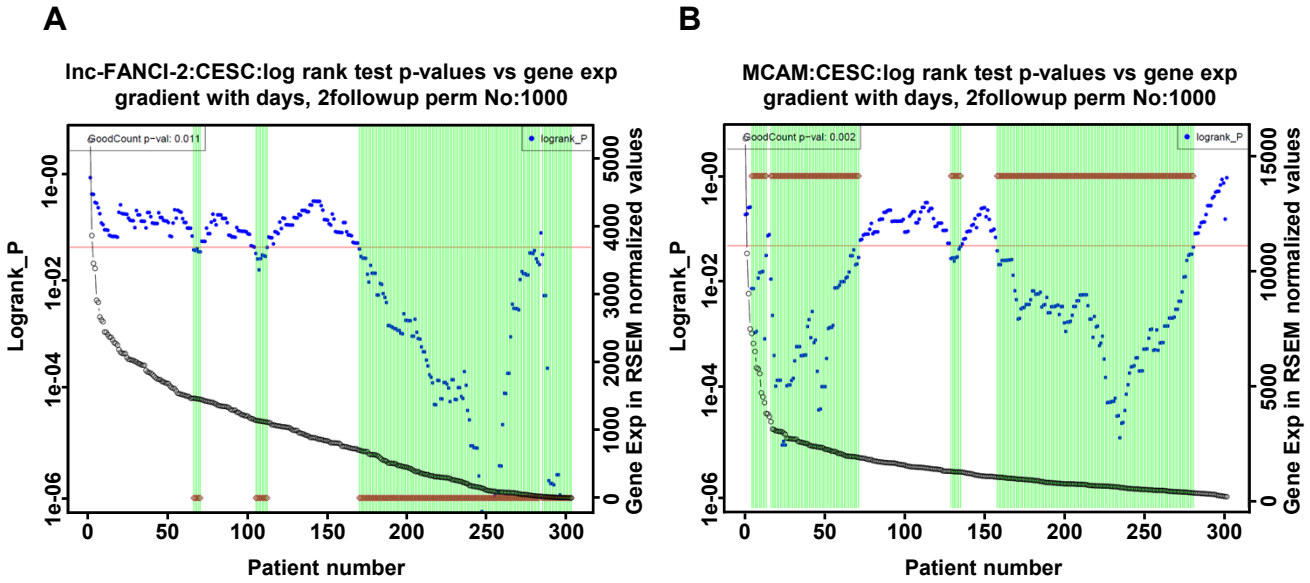

Fig. S8. Expression levels of lnc-FANCI-2 and MCAM are significantly associated with TCGA CESC (cervical squamous cell carcinoma) cancer patients' survival outcome. The expression of lnc-FANCI-2 (A) and of MCAM (B) along with survival of the same group of 304 cervical cancer patients were analyzed by our in-house GradientScanSurv pipeline (Yi et al 2018, PLoS One 13:e0207590). The **open grey circles** in each plot are ranked expression levels from high (left) to low (right) of lnc-FANCI-2 (A) and MCAM (B) from all patient samples as indicated by y-axis at the right side of the plot (in RSEM normalized value of RNAseq data). At each breaking point denoted by patient number (x-axis), the log rank test (y-axis at the left side of the plot) was performed between the higher expression group at the left side of the cut-point vs the lower expression group at the right side of the cut-point and the indicated log rank p-values (**blue dots**) are shown as at each cut-point at x-axis. The **horizontal red line** is the p=0.05 cutoff line for the log rank test p-values. If a log rank p-value (**blue dot**) at a cut-point is below the cutoff (p<0.05), there will be a **vertical green line** shown at the corresponding cut-point, indicative of a significant log rank test p-value, and also a **brown** diamond plotted either at the bottom part of the **vertical green line** (A) if higher expression of lnc-FANCI-2 led to less severe outcome (dying slower than the lower expressors), or at the top part of the **vertical green line** (B) if higher expression of MCAM led to more severe outcome (dying faster than the lower expressors).

The original GoodCount was defined as the number of significant log rank tests (the default significance level was set as 0.05) across all possible cut-points for the original dataset. We employed the bootstrap approach to permutate the data for 1000 times in this case. A similar procedure each time was performed like the original dataset and a permutated GoodCount was obtained for each permutated dataset. The GoodCount p-value was derived as the proportion of the times that the GoodCounts of permutated datasets were no less than that of the original dataset (Yi et al 2018, PLoS One 13:e0207590) and shown at the left top corner of each plot, 0.011 for lnc-FANCI-2 in panel A and 0.002 for MCAM in panel B. A significant GoodCount p-value (**blue dots** in both panels A and B) is indicative of significant association of the expression levels with the corresponding survival outcomes of the analyzed patient samples. Not shown in the panels A and B are the coxph p-value from univariant expression-based cox regression models (coxph p-value: derived by original gene expression values; or coxph p-value by rank: derived by corresponding ranks of gene expression values) and the cut-point-specific FDR and FDR2. FDR for each cut-point was defined as the portion of cases of permutated datasets that have log rank test p-values no higher than that of original dataset. FDR2 for each cut-point was defined as the portion of cases of permutated datasets that have log rank test p-values no higher than default setting of significance as 0.05.